JCB Journal of Cell Biology

ARTICLE

Rhythmic TDP-43 affects RNA splicing of USP13, resulting in alteration of BMAL1 ubiquitination

Jianlan Gu[1*], Mingming Yang[1*], Liti Zhang[1*], Yuxiao Liu[1], Ruolan Yan[1], Danmin Pan[2], Xiaowei Qian[2], Hanjing Hu[1], Dandan Chu[1], Chen Hu[3], Fei Liu[4], and Hengxiang Cui[5]

Circadian rhythm disorders are common characteristics of neurodegenerative diseases. The pathological aggregation of transactive response DNA-binding protein 43 (TDP-43) is associated with multiple neurodegenerative diseases, such as amyotrophic lateral sclerosis. However, the relationship between TDP-43 and circadian rhythm remains unknown. Here, we found that TDP-43 is rhythmically expressed both in vivo and in vitro. TDP-43 knockdown affected the expression of circadian genes, including *BMAL1*, *CLOCK*, *CRY1*, and *PER2*, and impaired autonomous circadian wheel behavior, cognitive functions, and balance abilities in mice. Furthermore, TDP-43 knockdown induced aberrant splicing of ubiquitin-specific peptidase 13 (USP13) and blocked USP13 rhythmic expression, enhancing the ubiquitination of BMAL1. Meanwhile, TDP-43 knockdown altered the rhythmic expression of phospho-AMPKα (Thr172) and platelet-type phosphofructokinase (PFKP), which may change cellular glucose uptake and ATP production. Our findings further the understanding of the role of TDP-43 dysfunction in circadian rhythm disruption in neurodegenerative diseases and provide new mechanistic evidence supporting the interaction between circadian rhythm disruption and neurodegeneration.

Introduction

As an internal rhythm in response to changes in the light–dark cycle from the external environment, the circadian clock is driven by interactions between internal biological clocks and external environmental signals such as light, temperature, and food intake (Patke et al., 2020). It affects most physiological processes including sleep, alertness, and cognitive performance. The core circadian clock in humans and mice contains a set of conserved clock proteins that form a transcriptional–translation feedback loop (TTFL) that mediates diurnal oscillations in gene expression. Brain and muscle Arnt-like protein-1 (BMAL1) forms a complex with circadian locomotor output cycle kaput (CLOCK) and binds to the E-box element in the promoters of period circadian protein (*PER*) and cryptochrome (*CRY*) genes. This leads to the rhythmic expression of PER, CRY, nuclear receptor subfamily 1 group D member 1 (NR1D1), and retinoic acid receptor–associated orphan receptor α (RORα) (Patke et al., 2020; Peng et al., 2022b; Richards and Gumz, 2013; Shrinivas et al., 2019).

Circadian rhythm disruption (CRD) is commonly observed in elderly individuals, particularly in those with neurodegenerative diseases, including Alzheimer's disease (AD) and Parkinson's disease (PD) (Musiek and Holtzman, 2016; Nassan and Videnovic, 2022; Ruan et al., 2021). Disruptions in circadian rhythms could be an initial sign of neurodegenerative disorders and increase the likelihood of developing neurodegeneration in individuals over the age of 60 who are otherwise healthy (Musiek and Holtzman, 2016). FUS, a heterogeneous nuclear ribonucleoprotein (hnRNP) closely linked to the onset of amyotrophic lateral sclerosis (ALS) and frontotemporal dementia (FTD), has the potential to regulate circadian rhythms (Jiang et al., 2018). It is transcriptionally regulated by NR1D1 and regulates PER and CRY expression (Jiang et al., 2018). The transactive response DNA-binding protein of 43 kDa (TDP-43) encoded by the *TARDBP* gene is another well-known ubiquitous conserved hnRNP associated with ALS and FTD. It plays important roles in transcription and RNA processing (Corbet et al., 2021; Flores et al., 2019; Polymenidou et al., 2011; Wang et al.,

[1]Department of Biochemistry and Molecular Biology, School of Medicine, Key Laboratory of Neuroregeneration and Ministry of Education of Jiangsu, Co-innovation Center of Neuroregeneration, NMPA Key Laboratory for Research and Evaluation of Tissue Engineering Technology Products, Nantong University, Nantong, China; [2]Department of Cell Biology, School of Life Sciences, Nantong University, Nantong, China; [3]Biomedical Translational Research Institute, School of Life Sciences and Medicine, Shandong University of Technology, Zibo, China; [4]Department of Neurochemistry, Inge Grundke-Iqbal Research Floor, New York State Institute for Basic Research in Developmental Disabilities, Staten Island, NY, USA; [5]Shanghai Key Laboratory of Psychotic Disorders, Brain Health Institute, National Center for Mental Disorders, Shanghai Mental Health Center, Shanghai Jiao Tong University School of Medicine, Shanghai, China.

*J. Gu, M. Yang, and L. Zhang contributed equally to this paper. Correspondence to Hengxiang Cui (lead contact): hengxiangc@qq.com; Fei Liu: fei.liu@opwdd.ny.gov; Chen Hu: chenhu2023@sdut.edu.cn; Jianlan Gu: ntgjlan@ntu.edu.cn.

2018). The aggregation of hyperphosphorylated, ubiquitinated, and truncated TDP-43 in neurons and glial cells is a common pathological feature of various neurodegenerative diseases including ALS, FTD, and AD (Chen and Mitchell, 2021; Josephs et al., 2014; Neumann et al., 2006; Prater et al., 2022). Cytoplasmic aggregation of TDP-43 leads to its nuclear depletion (McGoldrick and Robertson, 2023). Although TDP-43 stabilized the blue light receptor CRY1 by regulating the ubiquitin–proteasome system (Hirano et al., 2016), there is still scarce evidence supporting that TDP-43 controlling circadian rhythm function is involved in regulating the development of neurodegenerative diseases.

The utilization of glucose and energy produced in organisms exhibits a diurnal rhythm (Peng et al., 2022a; Womac et al., 2009). The hypothalamic suprachiasmatic nucleus (SCN) regulates the circadian oscillations in endogenous glucose production and extracellular adenosine triphosphate (ATP) accumulation (Marpegan et al., 2011; Peng et al., 2022a; Schmitt et al., 2018; Womac et al., 2009). AMP-activated protein kinase (AMPK) is the central regulator of energy sensing. Its expression and cellular localization also exhibit a rhythmic pattern (Lamia et al., 2009). Platelet-type phosphofructokinase (PFKP) is an enzyme that regulates the rate-limiting step of glycolysis and promotes fructose-6-phosphate (F6P) and ATP production, forming fructose-1,6-bisphosphate (FBP). PFKP regulates glucose oxidation by interacting with AMPK, affecting cellular energy and redox homeostasis and promoting cell survival under glucose starvation (Chen et al., 2022).

In this study, we found that the TDP-43 protein was expressed rhythmically in vivo and in cultured cells. Knockdown of TDP-43 changed the expression of rhythm genes, including *BMAL1*, *CLOCK*, *CRY1*, and *PER2*, the circadian rhythm function, and the cognitive and balance abilities of the mice. We found that TDP-43 regulated the deubiquitination of BMAL1 by affecting the variable splicing of ubiquitin-specific peptidase 13 (USP13) and expression of functional USP13, which impairs BMAL1 stability. Meanwhile, we found that the loss of the *Bmal1* gene in mice did not affect the rhythmic expression of TDP-43 in multiple tissues. This study has increased our understanding of the role of TDP-43 in circadian rhythm maintenance.

Results

TDP-43 is expressed rhythmically in vivo, and sleep deprivation alters its oscillated expression pattern

The intracellular loss and extracellular aggregation of TDP-43 are pathological characteristics of neurodegenerative diseases, including ALS, FTD, and AD (Josephs et al., 2014; Neumann et al., 2006). This may stabilize CRY1 in an F-Box and leucine-rich repeat protein (FBXL3)-dependent manner to maintain the circadian cycle (Hirano et al., 2016). However, whether this protein is regulated by circadian rhythms remains unclear.

We investigated the expression pattern of TDP-43 in mice brains over 24 h. C57BL/6 mice were photoperiodically synchronized for 4 wk before being sacrificed at four zeitgeist time (ZT) points, ZT0 (6 am), ZT6 (12 am), ZT12 (6 pm), and ZT18 (12 pm) (Fig. 1 A). Then levels of TDP-43 and BMAL1 in the cortex, hippocampus, and liver were analyzed by western blotting (Fig. 1 B). The results showed that the levels of TDP-43 were different at varies time points and displayed obvious circadian oscillation, which coincided with the level of BMAL1, a core circadian rhythmic protein, in the cortex, hippocampus, and liver of the mice (Fig. 1 B). Furthermore, immunofluorescence staining revealed a clear circadian rhythm in TDP-43 expression in the SCN, reaching its peak at ZT 20 (Fig. 1 F; and Fig. S1, A and B). These results strongly suggest that TDP-43 might be a novel rhythmic protein.

Sleep deprivation (SD) affects the expression of multiple core circadian rhythm genes. To investigate whether the rhythmic oscillation of TDP-43 was affected by sleep, similar to other rhythmic proteins, the mice were photoperiodically synchronized for 4 wk. They were then deprived of sleep for 6 h starting at ZT0, ZT6, ZT12, and ZT18, followed by sacrifice together with the non-sleep-deprived controls (Fig. S1 C). Immunoblots showed that the basal level of TDP-43 and the amplitude of oscillation were decreased in SD mice, with a trend similar to that of BMAL1 (Fig. S1 D). Using RT-qPCR, we found that the basal mRNA of *TARDBP* and the amplitude of oscillation were also decreased in the hypothalamus of SD mice (Fig. S1 E). These results suggest that the expression of *TARDBP* mRNA and the encoded TDP-43 are regulated by circadian rhythms.

TDP-43 knockdown affects the expression of core circadian genes in vitro

We further investigated whether TDP-43 affects the expression of circadian rhythm-related genes. Human neuroblastoma M17 cells were transfected with control vectors (NC) and gene-editing vectors targeting the *TARDBP* gene (TKD) followed by 2 h of serum-shock synchronization. Cells from each treatment group were collected at CT12 before being used for bulk RNA sequencing. Compared with the NC group, there were 1,005 upregulated and 945 downregulated genes in the TKD group (Fig. 2 A). Kyoto Encyclopedia of Genes and Genomes (KEGG) enrichment pathway analysis showed that in addition to enrichment of ALS-, AD-, and PD-related functional genes in the TKD group (Fig. 2 A), the genes related to ubiquitin-mediated protein degradation, AMPK signaling, and circadian activity (Fig. 2 A) were abundantly enriched in the TKD group, suggesting that TDP-43 may be involved in the regulation of ubiquitin-proteosome degradation of proteins, energy homeostasis, and circadian activity.

Based on our RNA sequencing (RNA-seq) data uploaded to the gene expression omnibus (GEO) database (GSE260737), TDP-43 knockdown mainly affected the abundance of sequencing reads assigned to *ARNTL/BMAL1*, *CLOCK*, *CRY*, and *PER* in M17 cells (Fig. 2 B). We further verified that TDP-43 knockdown led to an increase in the mRNA levels of *BMAL1*, *CLOCK*, and *NR1D1*, meanwhile, those of *PER2* and *CRY1* decreased in M17 cells at CT12 (Fig. 2 C). Therefore, TDP-43 knockdown likely affected the expression of multiple core circadian genes. In primary mouse brain fibroblasts (MBFs), TDP-43 knockdown significantly decreased the protein levels of BMAL1 at CT8, CT12, and CT16, CLOCK at CT16, CRY1 at CT12, CT16, CT20, and CT24, and PER2 at CT16 (Fig. 2 D). TDP-43 knockdown also significantly altered

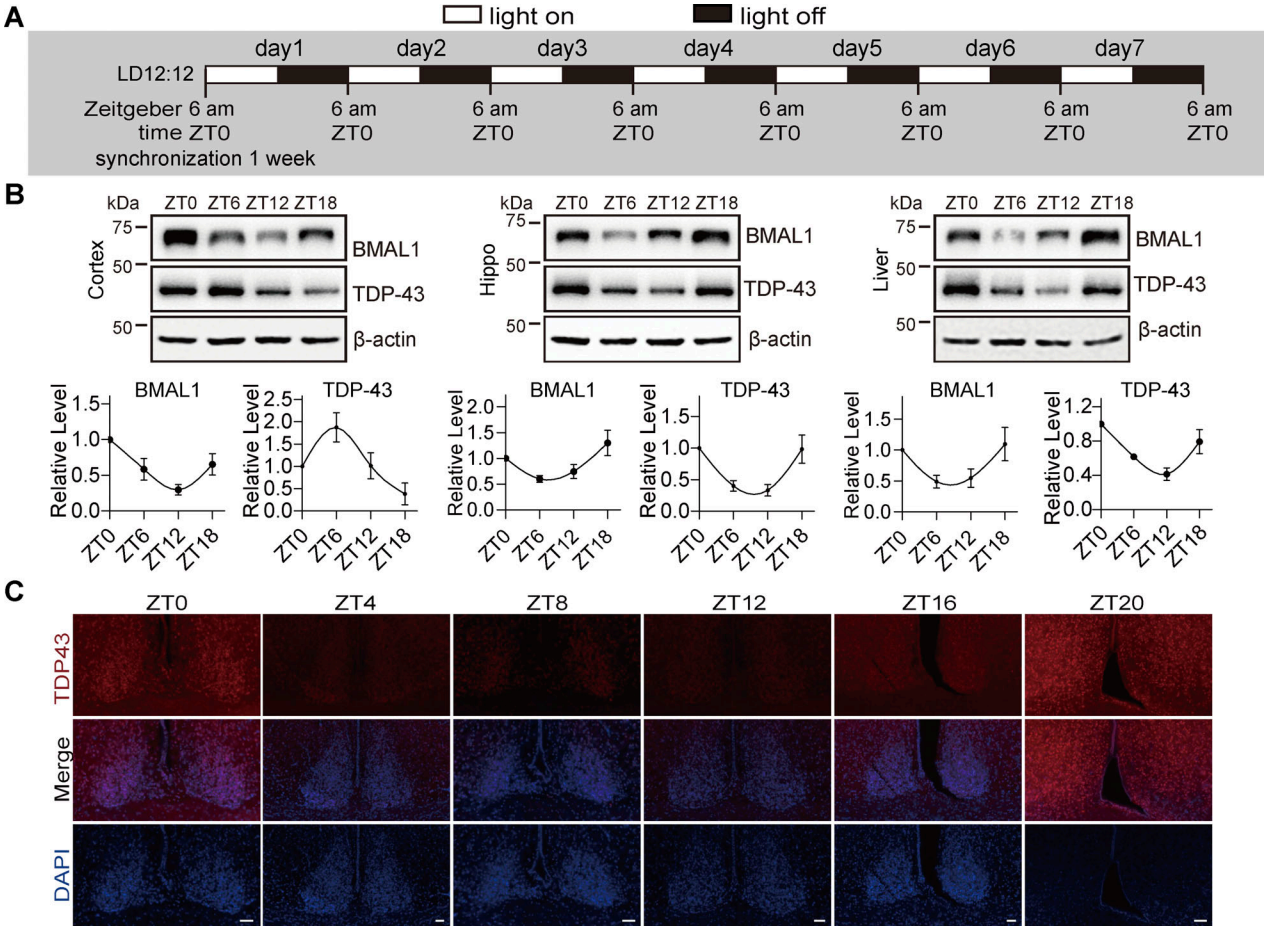

Figure 1. **TDP-43 is expressed rhythmically in vivo. (A)** The schematic of photoperiodic synchronized treatment of C57BL/6 mice. LD: light–dark, ZT: zeitgeber time. **(B)** The expression of BMAL1 and TDP-43 at indicated ZT time in the cortex, hippocampus, and liver were detected using western blotting and quantitated after densitometry. **(C)** The representative immunofluorescent staining of TDP-43 expression at indicated ZT time in the suprachiasmatic nucleus (SCN) of C57BL/6 mice. Immunostained sections (40 μm thickness per slice) were counterstained with TDP-43 antibody (red) and DAPI (blue). A total of five to six SCN regions were analyzed per mouse, with n = 5 mice at each time point. Scale bar: 200 μm. Data are presented as mean ± S.D. Source data are available for this figure: SourceData F1.

the periodic expression of BMAL1, CLOCK, PER2, and CRY1 (Fig. 2 D). Similar results were observed in HEK-293T cells depleted of TDP-43 (Fig. S2 A). Immunofluorescence staining showed that at the lowest point of circadian amplitude (CT0) and the highest point (CT12), M17 cells transfected with *TARDBP* gene-editing vectors (TKD) had significantly lower expression levels of PER2, CLOCK, BMAL1, and CRY1 than the NC group (Fig. 2 E). The ectopic expression of human TDP-43 in synchronized TDP-43-knockdown HEK-293T cells restored the expression of PER2, CLOCK, and BMAL1 (Fig. S2 B). These results further support that TDP-43 regulates the expression of rhythm proteins.

BMAL1 is generally considered as the key gene of the molecular clock because the knockdown of BMAL1 down-regulates the expression of other rhythm genes (Bolsius et al., 2021). Consistently, we found that the knockdown of BMAL1 significantly decreased the expression of PER2, CLOCK, and CRY1, but did not affect the expression of TDP-43 at both mRNA and protein levels (Fig. S2 C), suggesting that TDP-43 may act upstream of BMAL1.

TDP-43 knockdown changes the expression of core circadian proteins in the hypothalamus and induces circadian period change in mice

SCN is the principal circadian clock in the brain. Therefore, we investigated whether TDP-43 knockdown affects the expression of core rhythmic genes in the SCN of mice. Control and TDP-43 knockdown adenoassociated virus (AAV) were intracerebroventricularly (icv) injected bilaterally into 8-wk-old C57BL/6 mice. 3 wk after injection, the mice were subjected to a 12/12 h light/dark (LD) cycle for 1 wk and sacrificed at ZT0, ZT5, ZT10, ZT15, and ZT20 (Fig. 3 A).

We first investigated whether TDP-43 knockdown affected circadian rhythm behavior and cognition in vivo. We evaluated the effect of TDP-43 knockdown on wheel-running activity, which correlated with circadian rhythm in mice. After familiarization with the running wheels for 3 wk in 12/12 h light–dark (LD), followed by 3 wk of complete dark–dark (DD) exposure, the mice in both control (CON) and TDP-43 knockdown (shTDP-43) groups retained free-running rhythms in DD (Fig. 3 A). The circadian periods, determined by analyzing the recorded data of

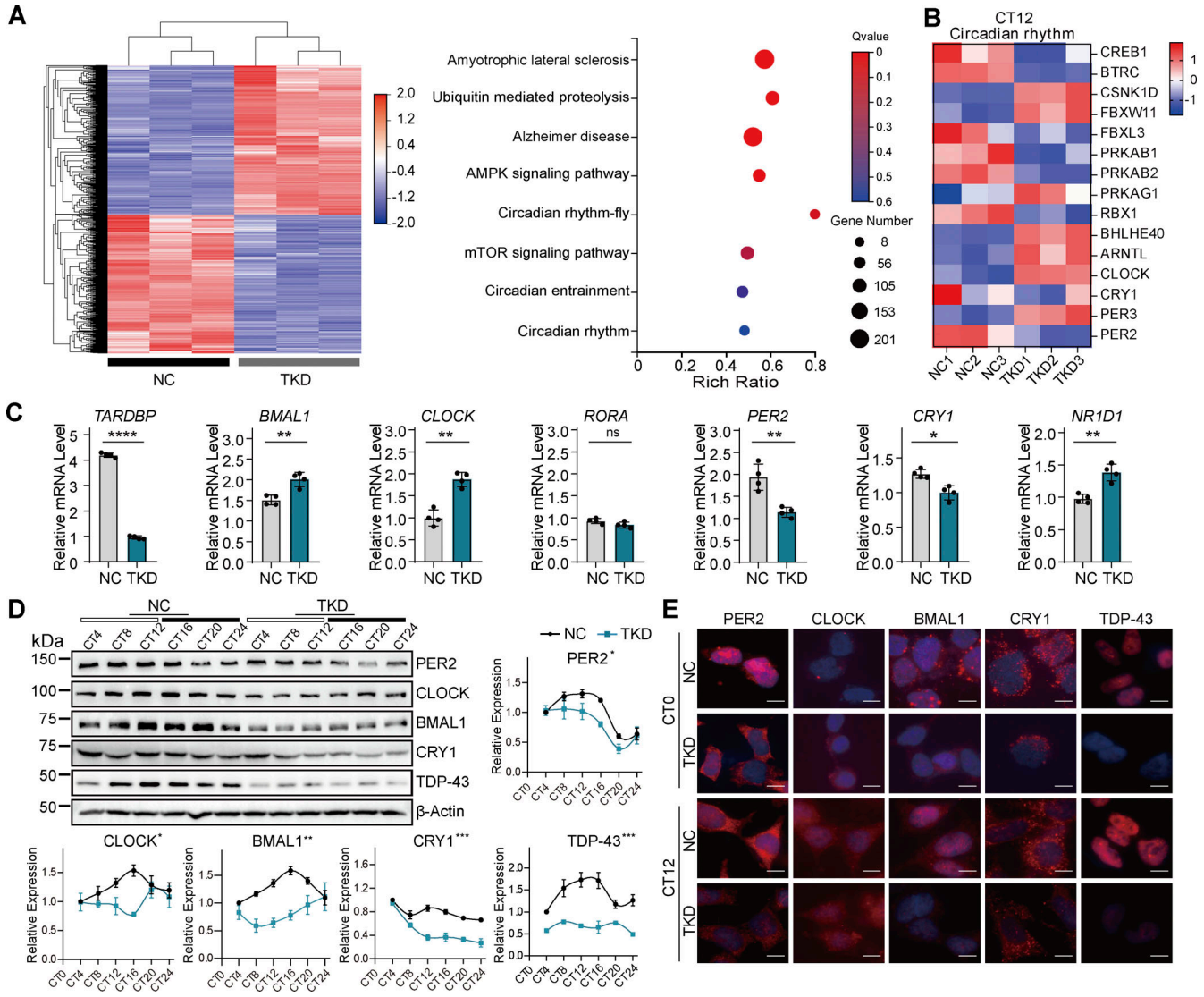

Figure 2. **TDP-43 knockdown affects the expression of core circadian genes in vitro. (A)** M17 cells were transfected with gene-editing vectors targeting *TARDBP* (TKD) or control vectors (NC) for 72 h. They were then synchronized by culture with 50% horse serum DMEM for 2 h and serum-free DMEM for 34 h. The cells were lysed in TRIzol and sent to Huada Gene Company for transcriptome sequencing. Left is the upregulated and downregulated genes in the TKD group (n = 3, |log2FC| ≥1, Qvalue ≤0.05), and the KEGG enrichment pathway analysis is shown on the right. Red, upregulated genes; blue, downregulated genes. **(B)** Heat maps represent the significantly downregulated or upregulated rhythm genes in two groups. **(C)** The mRNA levels of *BMAL1*, *CLOCK*, *RORA*, *PER2*, *CRY1*, *NR1D1*, and *TARDBP* in two groups were detected using RT-qPCR and statistically analyzed by unpaired t test (n = 4). **(D)** Mouse brain fibroblasts (MBFs) were transfected with LentiCRISPR v2/TDP-43$_{KO}$ (TKD) and control vectors (NC) and then synchronized and collected every 4 h at CT4, CT8, CT12, CT16, CT20, and CT24. The cell lysates were analyzed using western blotting and statistically analyzed with comparison by two-way RM ANOVA. **(E)** M17 cells were transfected with LentiCRISPR v2/TKD for 48 h and then synchronized for 24 h (CT0) or 36 h (CT12), and immunostained with indicated antibodies (red) and DAPI (blue). Scale bar, 20 μm. Data are presented as mean ± S.D. *P < 0.05; **P < 0.01; ***P < 0.001; ****P < 0.0001. Source data are available for this figure: SourceData F2.

animal wheel activity during the dark–dark cycle, in shTDP-43 infected (shTDP-43) mice were significantly shorter than those in the control virus-infected (CON) mice (Fig. 3, A and B). In the open field test, there was no difference between the control and TDP-43 knockdown mice in the distance and duration of movement (Fig. 3 C). This indicated that TDP-43 knockdown did not alter the spontaneous activity of animals and the observed differences in circadian behavior between the control and TDP-43 knockdown mice were not because of the changes in the locomotor activity from TDP-43 knockdown. These findings suggest that a reduction in TDP-43 alters the circadian rhythm in mice.

Motor learning and coordination of mice were assessed using an accelerating rotarod apparatus in which the latency and rate of fall were decreased in shTDP-43 virus-infected mice (Fig. 3 D). This indicated that TDP-43 knockdown might affect motor coordination ability. During the fourth training day in the Morris water maze task, shTDP-43 virus-infected mice took more time to locate the escape platform (Fig. 3 E). This indicated that the spatial learning and memory of the mice may be impaired.

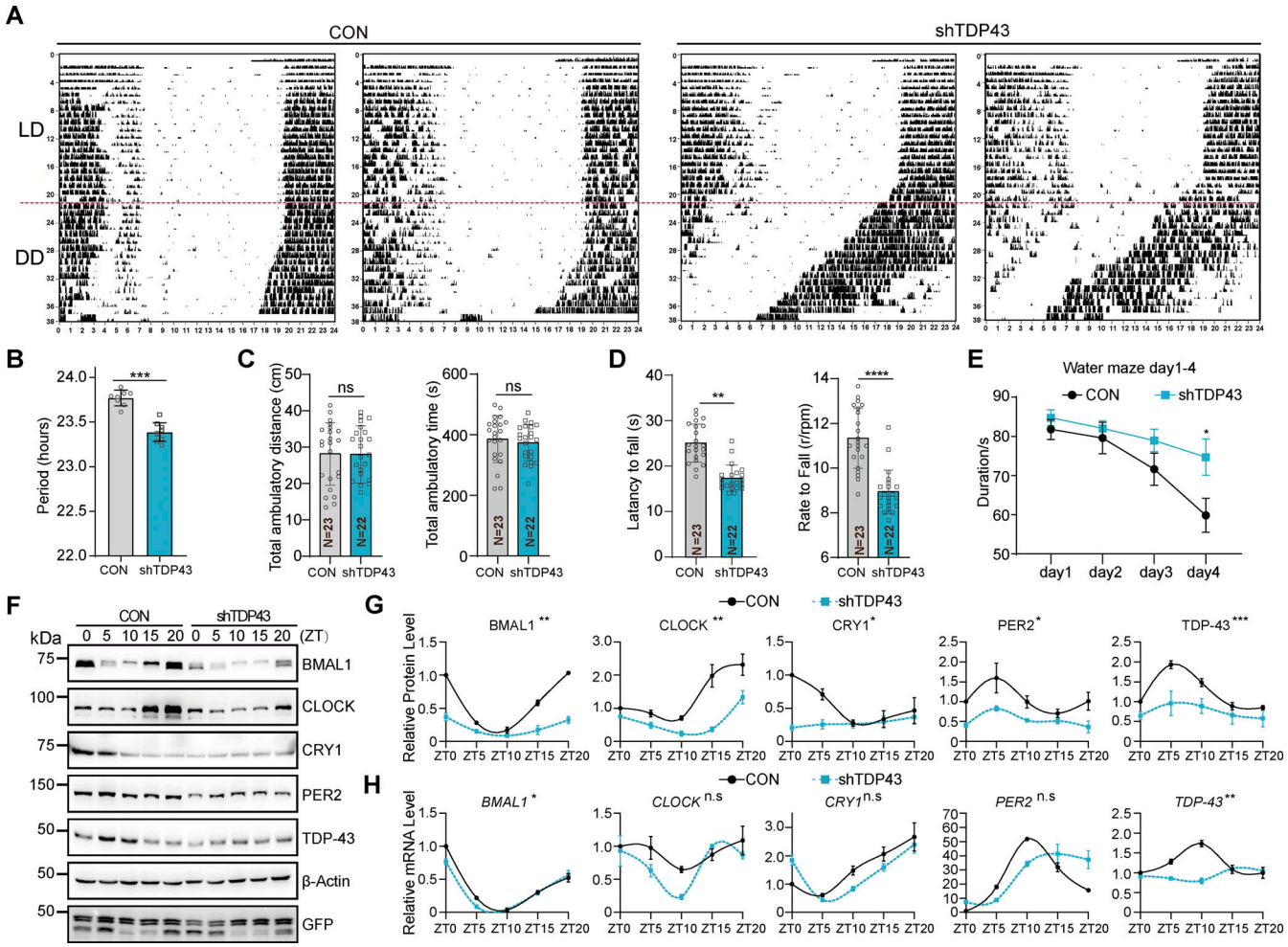

Figure 3. **TDP-43 knockdown changes the expression of core circadian proteins in the hypothalamus and induces circadian period change in mice.** 8-wk-old C57BL/6 mice were injected with control AAV (CON) or AAV carrying TDP-43 shRNA (shTDP-43) tagged with GFP into the ventricles bilaterally. 3 wk later, the mice were subjected to light–dark (LD) synchronization for 1 wk and acclimated to running wheels for 3 wk in 12/12 h LD. This was followed by 3 wk of complete dark–dark (DD) exposure and other behavior analysis. LD: light–dark, DD: dark–dark. **(A and B)** The representative actograms of the wheel-running records (A) and quantification (B). The horizontal (hour) and vertical (day) axes represented time and days, respectively. Red dotted lines showed the start day for constant darkness. **(C)** The total distance traveled, immobility time, mean speed, time spent in the central zone, number of entries into the central zone, and the mean distance from the central zone of the mice were recorded for the shTDP-43 and CON mice in the open field test. **(D)** Motor learning and coordination of the mice was assessed using a rotarod test. **(E)** The swimming speed, the first latency to the platform (target) zone, and the distance traveled until the first reaching the target zone were measured using the Morris water maze test. During the training days, the time of the mice took to reach the escape platform (latency) was recorded. The quantitation of the result was compared and statistically analyzed. **(F and G)** The mice were euthanized at five time points, ZT0, ZT5, ZT10, ZT15, and ZT20 (n = 3). The hypothalamus was dissected and analyzed using immune blots with indicated antibodies (F) with each band quantitated and compared by two-way RM ANOVA (G). **(H)** The mRNA level of circadian genes in the hypothalamus of the mice was detected using RT-qPCR, with quantitation and comparing by two-way RM ANOVA. Data are presented as mean ± S.D. (n = 3). *P < 0.05; **P < 0.01; ***P < 0.001; ****P < 0.0001. n.s, no significance. Source data are available for this figure: SourceData F3.

Western blotting showed that TDP-43 knockdown by shRNA downregulated the protein expression of BMAL1, PER2, CLOCK, and CRY1 (Fig. 3 F). BMAL1 protein expression was significantly decreased by TDP-43 knockdown at ZT0, ZT15, and ZT20, CLOCK at ZT15 and ZT20, CRY1 at ZT0 and ZT5, and PER2 at ZT0, ZT5, and ZT20 (Fig. 3 G). The effect of TDP-43 knockdown on the periodic expression patterns of circadian proteins (Fig. 3 F) was consistent with observations in the in vitro cellular model (Fig. 2 D). The changes in the mRNA expression patterns of circadian genes caused by TDP-43 knockdown in mouse brains (Fig. 3 H) were similar to those observed in an in vitro cellular model (Fig. 2 C).

TDP-43 regulates the ubiquitination of BMAL1

Bulk RNA sequencing showed that genes related to ubiquitin-mediated proteolysis were enriched in the TKD group (Fig. 2 A). Moreover, TDP-43 knockdown suppressed BMAL1 protein expression and promoted its mRNA expression, leading us to first evaluate whether TDP-43 regulated the stability of BMAL1 and other circadian rhythm proteins. Using cycloheximide (CHX) to inhibit protein synthesis in M17 cells showed that the degradation of BMAL1, CLOCK and CRY1, but not that of PER2, was significantly lower in the TKD group than in the control group (Fig. 4, A and B). MG132, a ubiquitin–proteasome specific inhibitor, considerably blocked the degradation of BMAL1 in M17

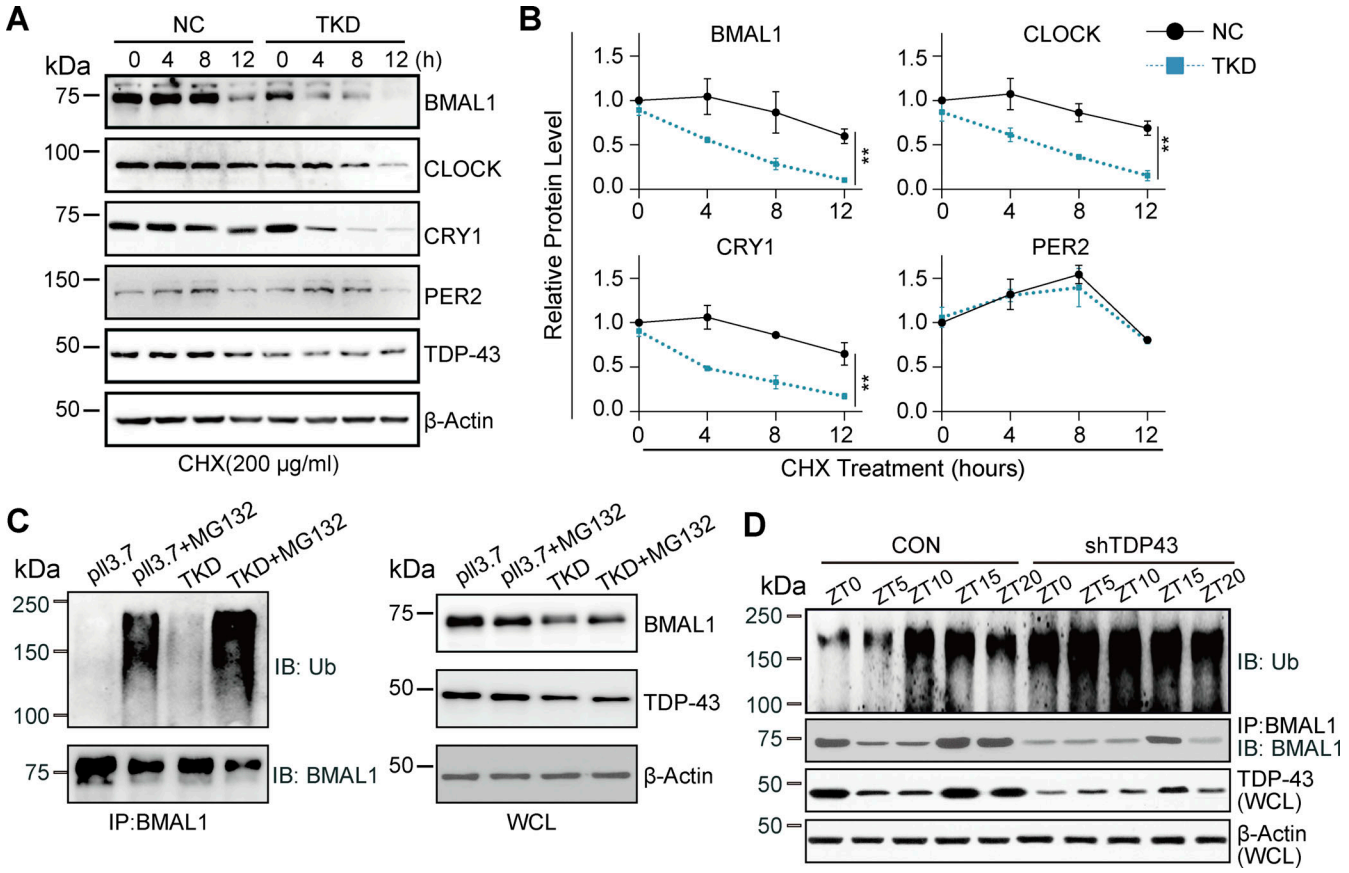

Figure 4. **TDP-43 regulates the ubiquitination of BMAL1 which modulates BMAL1 stability. (A and B)** M17 cells were infected with PX458/TDP-43KO (TKD). 48 h later, the cells were synchronized by being cultured in DMEM/50% horse serum for 2 h, and then DMEM/1% FBS for 22 h. They were then treated with CHX (200 μg/ml) at CT8. The cell lysates were extracted every 4 h (0, 4, 8, and 12 h), analyzed by western blotting (A), and quantitated by comparing by two-way RM ANOVA (B). **(C)** HEK-293T cells were transfected with TKD for 48 h and immunoprecipitated with anti-BMAL1 and analyzed using western blotting. WCL: whole cell lysate. **(D)** Cortex homogenates from control AAV (CON) or AAV carrying TDP-43 shRNA (shTDP-43) injected C57BL/6 mice collected at several zeitgeber times, ZT0, ZT5, ZT10, ZT15, and ZT20, were immunoprecipitated with anti-BMAL1 and analyzed by western blotting with indicated antibodies. Data are presented as mean ± S.D. (n = 3). **P < 0.01. Source data are available for this figure: SourceData F4.

cells (Fig. 4 C). The ubiquitination of BMAL1 was increased by TDP-43 knockdown (Fig. 4 C), directly supporting the hypothesis that the knockdown of TDP-43 affected the ubiquitination of BMAL1.

We also performed immunoprecipitation with cortex homogenates from shTDP-43 virus-infected mice collected at several zeitgeber times (ZT0, ZT5, ZT10, ZT15, and ZT20) using an anti-BMAL1 antibody and performed to immunoblot analysis (Fig. 4 D). Compared with the control group, we observed an increase in the ubiquitination level of BMAL1 in the TDP-43 knockdown group. Our findings suggest that TDP-43 regulates the ubiquitination of BMAL1 by modulating its protein stability (Fig. 4 D).

TDP-43 regulates the expression of USP13, resulting in alteration of BMAL1 ubiquitination

Then we wanted to know by which TDP-43 regulates the ubiquitination of BMAL1. The RNA-seq results (Roczniak-Ferguson and Ferguson, 2019) showed that the deubiquitinated ubiquitin-specific peptidase 13 (USP13) was altered by TDP-43 knockdown (Fig. 5 A). We confirmed that *USP13* mRNA expression was decreased by TDP-43 knockdown and could be restored by the ectopic expression of wild-type TDP-43 in TDP-43 knockdown M17 cells (Fig. 5 B). USP13 was expressed periodically, and the periodicity disappeared after TDP-43 knockdown (Fig. 5 C).

We previously reported that TDP-43 regulates the alternative splicing of tau exon 10 and promotes tau instability (Gu et al., 2017a, 2017b). TDP-43 contains tandem RNA recognition motifs and acts as an alternative splicing regulator by binding to long UG-rich RNA sequences to modulate gene splicing (Lukavsky et al., 2013). Intron 1 of *USP13* contains UG-rich RNA sequence (Fig. 5 D). Analysis of the differences in the sequence readers of *USP13* splicing revealed a moderate difference between the vector control and TDP-43 knockdown groups. We found one UG-rich RNA sequence localized in intron 1 of the *USP13* pre-mature mRNA (Fig. 5 D). Therefore, TDP-43 may inhibit UG-rich RNA splicing. Using RT-PCR, we confirmed that TDP-43 knockdown led to more intron sequences being spliced into *USP13* mRNA (Fig. 5 D). This could potentially elucidate the reason for the diminished normal mRNA formation of *USP13* upon TDP-43 knockdown, leading to altered USP13 expression. Reducing the expression of USP13 in HEK-293T cells led to a

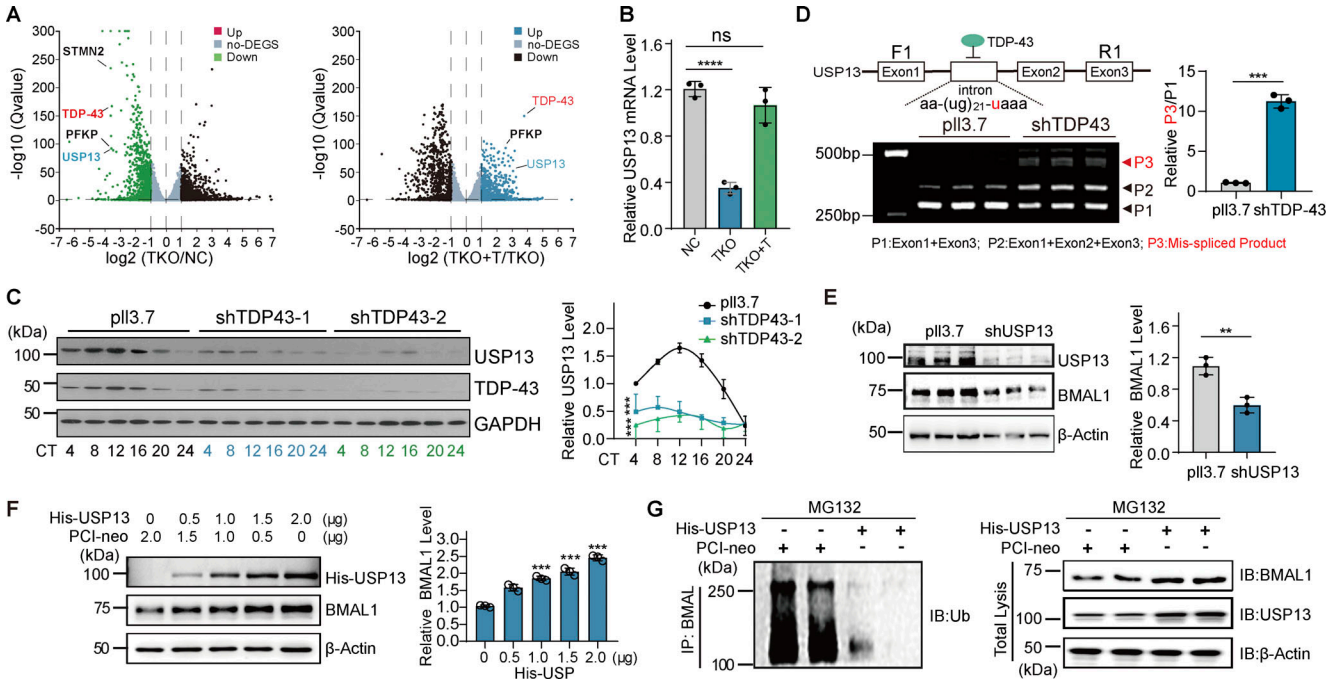

Figure 5. **TDP-43 regulates the expression of USP13. (A)** *USP13* was found from two sets of RNA-seq data (Roczniak-Ferguson and Ferguson, 2019). **(B)** HEK-293T cells were transfected with PX458/TDP-43$_{KO}$ (TKD) and HA-TDP-43 24 h later. The cells were collected 48 h later and RNA was extracted and performed to RT-qPCR. ns, no significance. **(C)** HEK-293T cells were transfected with pLL3.7, shTDP-43$_1$, and shTDP-43$_2$. The cells were collected at different CT and analyzed using western blotting and quantitated by comparing by two-way RM ANOVA. **(D)** M17 cells were transfected with PX458/TKD, and RNA was extracted 48 h later. The splicing products of *USP13* were analyzed using RT-PCR and the ratio of P3/P1 was calculated. **(E)** HEK-293T cells were transfected with shUSP13 for 48 h, and the cell lysates were analyzed using western blotting and quantitated. **(F)** HEK-293T cells were transfected with 0, 0.5, 1, 1.5, and 2 μg His-USP13 for 48 h, and the cell lysates were analyzed using western blotting, with the relative expression of BMAL1 quantitated in each treatment. **(G)** HEK-293T cells were transfected with shTDP-43 for 24 h and then transfected with His-USP13 and treated with MG132 (10 μM) for 12 h. The cells were immunoprecipitated with anti-BMAL1 and analyzed using western blotting. Data are presented as mean ± S.D. (n = 3). The unpaired t test was used in comparisons of B and D–F. **P < 0.01; ***P < 0.001; ****P < 0.0001. ns, no significance. Source data are available for this figure: SourceData F5.

significant decrease in BMAL1 level (Fig. 5 E). Meanwhile, introducing an increasing amount of USP13 into HEK-293T cells resulted in a dose-dependent increase in BMAL1 protein level (Fig. 5 F). Thus, we recognized that TDP-43 knockdown decreased the mRNA and protein expression of USP13, thereby affecting the protein level of BMAL1 in cells. Using MG132 to inhibit the ubiquitin–proteasome process showed that ectopic expression of USP13 almost completely removed the ubiquitin modification from BMAL1 and increased BMAL1 protein level in cells with TDP-43 knockdown (Fig. 5 G). These findings suggest that USP13 might affect BMAL1 protein level by modulating the ubiquitination of BMAL1.

The immunoprecipitation assay showed that anti-USP13 captured BMAL1 and also anti-USP13 captured BMAL1 from M17 cell lysates (Fig. 6 A). In vitro–purified GST-tagged USP13 protein interacted with His-tagged BMAL1 (Fig. 6 B). Overexpression of wild-type USP13 in HEK-293T (Fig. 5 F) and M17 cells (Fig. 6 C) increased the protein level of BMAL1 in a dose-dependent manner, but overexpression of mutant USP13 (USP13 CA) (Fang et al., 2017) did not increase BMAL1 expression (Fig. 6 C), and we verified that USP13 knockdown decreased the cellular protein levels of BMAL1 in M17 cells (Fig. 6 D). By using CHX to inhibit eukaryotic translation, we found that USP13 knockdown accelerated the decrease of BMAL1 protein level in M17 cells (Fig. 6 E). To determine whether USP13 deubiquitinates BMAL1, HEK-293T cells were transfected with BMAL1, USP13 (wild type), or the enzyme-deficient mutant USP13 C345A (USP13 CA) and 6×His-ubiquitin. The ubiquitination level of BMAL1 was determined by Ni-NTA purification of proteins conjugated to 6×His-ubiquitin and BMAL1 by western blotting. We found that wild-type USP13, but not USP13 CA, deubiquitinated BMAL1 (Fig. 6 F). In USP13-knockdown M17 cells, wild-type USP13 expression, not the mutant USP13, elevated the protein level of BMAL1 (Fig. 6 G). We also found that in TDP-43-knockdown M17 cells, wild-type USP13 elevated the protein level of BMAL1, but not the mutant USP13 (Fig. 6 H). In mice infected with *TARDBP* interference virus, restoring the expression of wild-type USP13 reduced the ubiquitination of BMAL1 in the hypothalamus but not the mutant USP13 (Fig. 6 I). Thus, we believe that USP13 directly interacts with BMAL1 and regulates the ubiquitination of BMAL1 (Fig. 5 G and Fig. 6 I).

The rhythmic expression of TDP-43 remains unchanged in multiple tissues of *BMAL1* knockout mice

BMAL1 is a core component of the mammalian circadian clock, and its absence leads to the loss of circadian behaviors (Partch et al., 2014; Ray et al., 2020). Since TDP-43 regulates

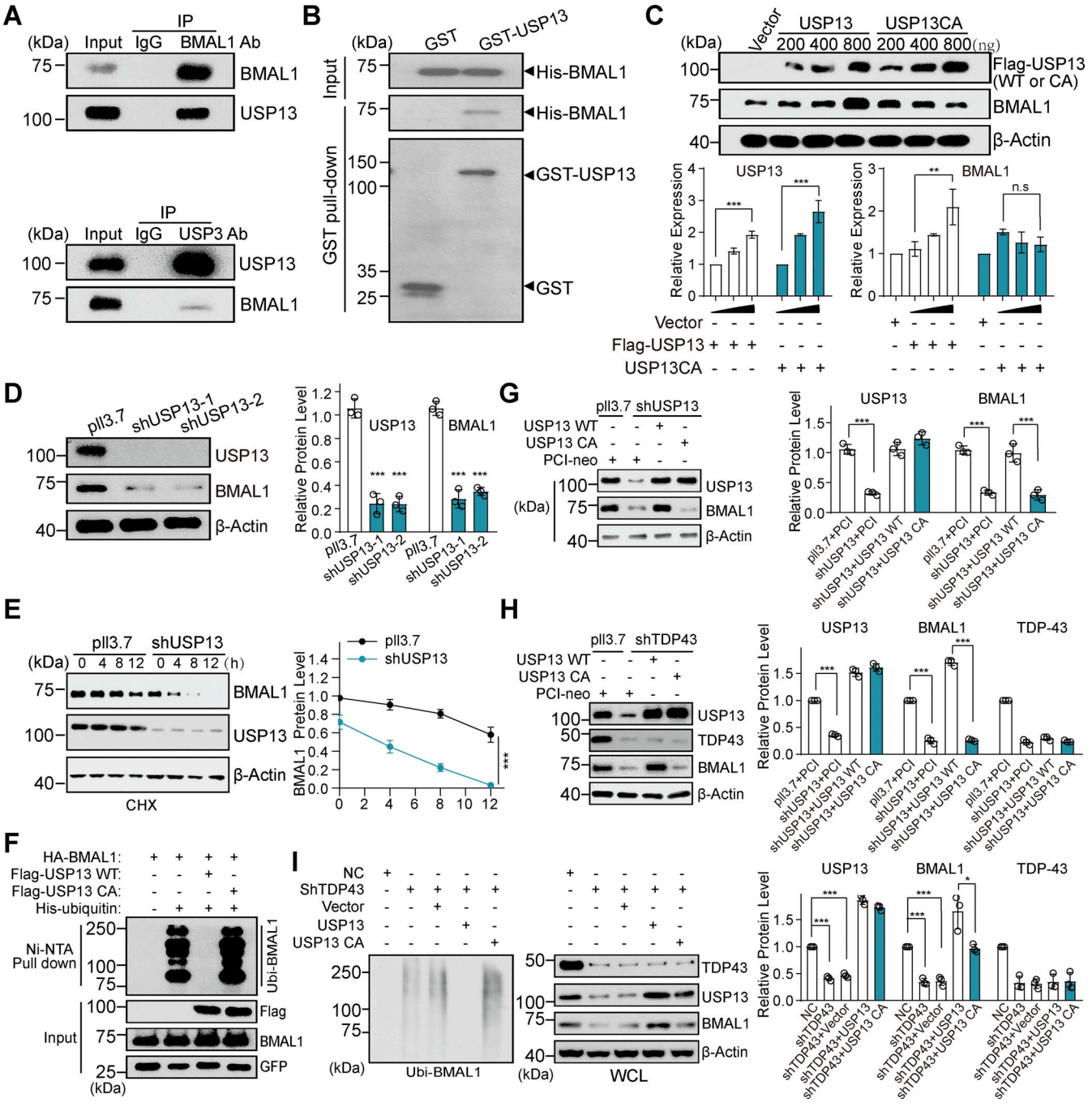

Figure 6. **USP13 physically interacts with BMAL1 to regulate its ubiquitination. (A)** M17 cell lysate was immunoprecipitated with anti-BMAL1 (Up panel), or anti-USP13 (Down panel), and analyzed by western blotting with anti-USP13. **(B)** Bacterial-purified GST or GST-USP13 was incubated with His-BMAL1 isolated from *E. coli*, and the GST pull-down assays were performed followed by western blotting analysis using anti-BMAL1. **(C)** M17 cells were transfected with pcDNA3.1 (Vector), pcDNA3.1/Flag-USP13 (USP13), or pcDNA3.1/Flag-USP13 C345A (USP13 CA) at indicated doses for 24 h, the cell lysates were analyzed by western blotting, and quantitated. **(D)** M17 cells were transfected with shUSP13-1 or shUSP13-2 for 48 h, and the cell lysates were analyzed by western blotting, and quantitated. **(E)** M17 cells were transfected with control (pll3.7) or shUSP13, then treated with cycloheximide (CHX) for the indicated time, and the cell lysates were analyzed by western blotting with quantitation and compared by two-way RM ANOVA. **(F)** HEK-293T cells were transfected with indicated ectopic vectors for 48 h, and the cell lysates were immunoprecipitated with Ni-NTA beads, then analyzed by western blotting with BMAL1 antibody. The whole cell lysate of each treatment was also used to determine the expression of indicated proteins. **(G and H)** M17 cells were transfected with indicated ectopic vectors and analyzed by western blotting, and quantitated. **(I)** 8-wk-old C57BL/6 mice were icv-injected with indicated AAV virus bilaterally. 18 days later, the hypothalami of mice were isolated before being subjected to detect the ubiquitin-conjugated BMAL1 and indicated protein expression in the tissue, with the expression of indicated proteins quantitated in each group (n = 3). The unpaired t test was used in comparisons in C, D, and G–I. *P < 0.05; **P < 0.01; ***P < 0.001. n.s, no significance. Source data are available for this figure: SourceData F6.

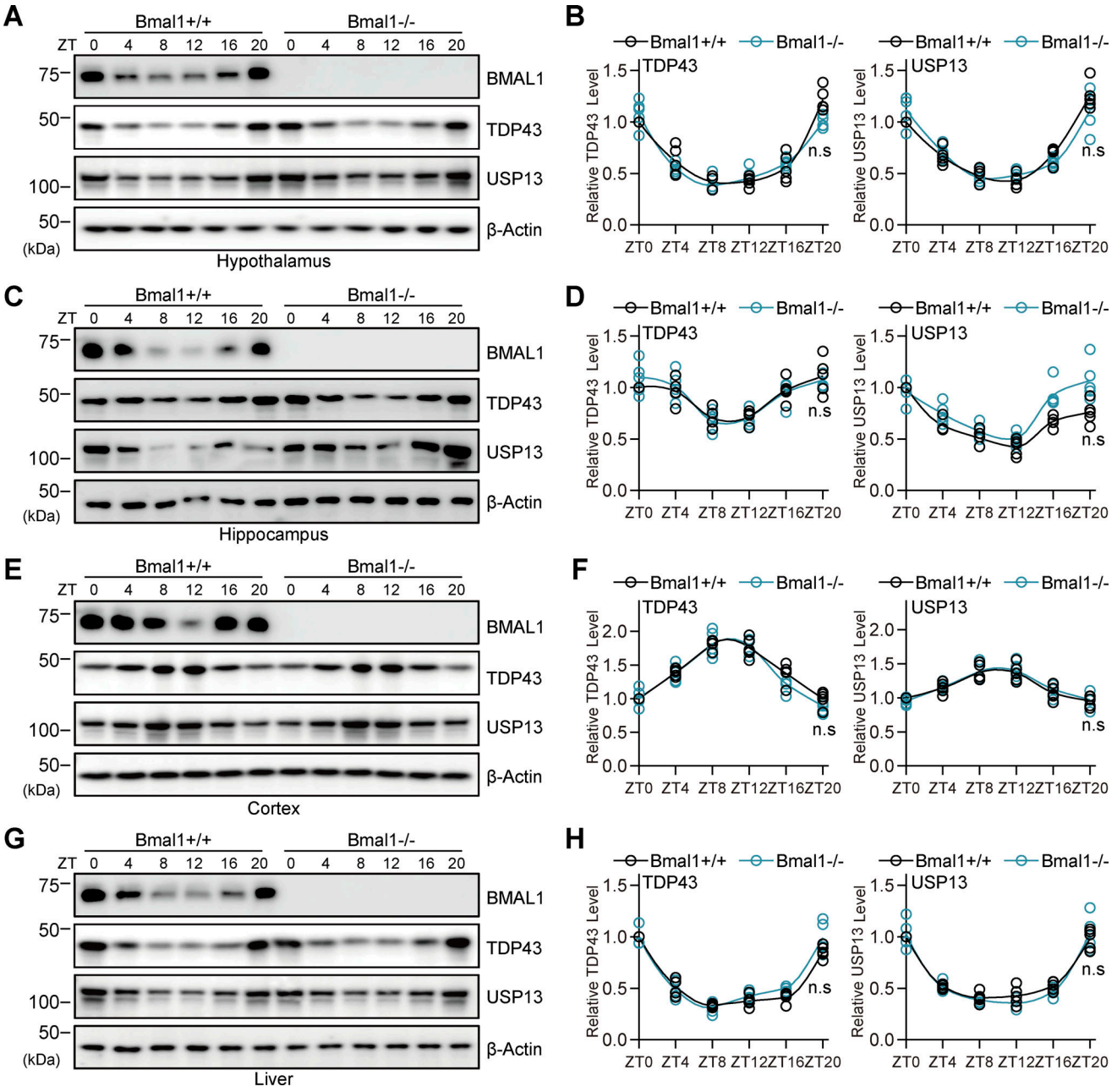

Figure 7. **Rhythmic expression of TDP-43 in multiple tissues of *Bmal1* knockout mice. (A–H)** The hypothalamus, hippocampus, cortex, and liver were isolated from wild type (*Bmal1*$^{+/+}$) (n = 30) and *Bmal1* knockout (*Bmal1*$^{-/-}$) (n = 30) mice at age of 4 wk, before being sacrificed at six zeitgeist time (ZT) points, including ZT0 (6 am), ZT4 (10 am), ZT8 (14 pm), ZT12 (18 pm), ZT16 (22 pm), and ZT24 (2 am). For each genotype, five animals were sacrificed at each zeitgeist time with each tissue lysed into samples followed by western blotting to determine the expression of BMAL1, TDP-43, and USP13 proteins. The representative blots were shown (A, C, E, and G), with the relative expression of five samples at each zeitgeist time quantitated were compared by two-way RM ANOVA (B, D, F, and H). Data are presented as mean ± S.D. (n = 5). n.s, no significance. Source data are available for this figure: SourceData F7.

the rhythmic expression of BMAL1 protein and its knockdown causes phenotypic changes in rhythms, we are curious whether BMAL1 affects the rhythmic expression of TDP-43.

The results revealed that in 4-wk-old mice with *Bmal1* knockout, we did not observe significant changes in the rhythmic expression pattern of TDP-43 in the hypothalamus, cortex, hippocampus, and liver (Fig. 7, A–H). By western blotting, we found rhythmic oscillation of USP13 expression in M17 cells (Fig. S3). In the hypothalamus, cortex, hippocampus, and liver of 4-wk-old wild-type mice, we observed rhythmic oscillation of the protein level of USP13, although the amplitude of the oscillations was not massive; besides, the oscillations were not affected by *BMAL1* knockout (Fig. 7, A–H).

These findings support that USP13 expression also exhibits a rhythmic pattern, and USP13 interacts with BMAL1 to regulate ubiquitination of BMAL1, thereby affecting the protein level of BMAL1 in cells.

TDP-43 and BMAL1 regulate the rhythmic expression of activated AMPK and PFKP

The circadian system controls glucose and energy metabolism in humans. TDP-43 truncation has been shown to induce metabolic reduction of metabolic intermediates that supply glycolysis and the tricarboxylic acid cycle (TCA), and TDP-43 proteinopathy also induced metabolic alterations, including the TCA cycle, in models of ALS (Loganathan et al., 2022; Maksimovic et al., 2023). However, there is insufficient data regarding the impact of TDP-43 knockdown on the TCA cycle and its role in regulating cellular energy production in the TCA cycle.

Here, we found that in metabolomics, TDP-43 knockdown led to a decrease in multiple glycolytic and TCA cycle intermediates including F6P, glucose-6-phosphate, FBP, phosphoenolpyruvate, 3-phospho-D-glyceric acid (3-PGA), pyruvate, and lactate (Fig. S4 A). TDP-43 knockdown also decreased versatile energy production intermediates (Fig. S4 B). RNA-seq analysis (GSE260737) showed that the sequence reads of multiple glycolysis- and TCA-related genes were also altered by TDP-43 knockdown (Fig. 2 A). This supports that TDP-43 may control cellular glycolysis and the TCA cycle. For glucose can provide energy to organisms through glycolysis and TCA cycle, we investigated whether TDP-43 knockdown affects cellular glucose uptake and the expression of glucose transporters (GLUTs). TDP-43 knockdown led to a decrease in the cellular glucose uptake capacity (Fig. S4 C). TDP-43 knockdown resulted in decreased expression of GLUT2 and GLUT3, which might explain the reason for TDP-43 knockdown attenuating cellular glucose uptake (Fig. S4 D).

Given that TDP-43 knockout decreased ATP production in metabolomics, and AMPK, which is also rhythmic (Lamia et al., 2009), is the most important molecule in organisms that senses energy levels and regulates metabolic homeostasis, we also examined whether the TDP-43–BMAL1 axis regulates AMPK signaling. TDP-43 and BMAL1 knockdown significantly induced AMPK activation at ZT4 and ZT8 and altered the pattern of AMPK activation over time (Fig. 8, A and B). In the TDP-43 knockdown cells, ectopic expression of BMAL1 or USP13 significantly restored ATP levels (Fig. S4 F). This supported that TDP-43 knockdown-induced ATP attenuation is dependent on cellular BMAL1 and USP13 levels. These findings let us deduce that TDP-43 could regulate glucose transporter expression and AMPK signaling in neurons, controlling glucose uptake, cellular glycolysis, and energy production in neuronal cells.

Based on the RNA-seq and metabolomic results, we further evaluated the effect of TDP-43 knockdown on the expression of glycolysis-related proteins. TDP-43 knockdown significantly decreased the expression of the glycolysis-related proteins PFKP, HXK1, and LDHA (Liu et al., 2017; Zheng et al., 2016) (Fig. S5 A). This result is consistent with the findings of a previous metabolomic study on the effects of TDP-43 on glycolysis and TCA (Fig. S4, A and B). We also found that PFKP was expressed rhythmically and TDP-43 knockdown led to the disappearance of periodic expression patterns (Fig. 8 C). In the promoter of *PFKP*, we found multiple conserved BMAL1 binding consensus sites and PFKP expression may be regulated by BMAL1. We also found that BMAL1 knockdown decreased PFKP protein expression (Fig. S5 B). According to the chromatin immunoprecipitation assay, BMAL1 could regulate the transcriptional activity of *PFKP* by directly binding to the promoter of the *PFKP* gene (Fig. S5 C). These results suggest that the TDP-43–BMAL1 signaling may regulate the rhythmic expression of activated AMPK and PFKP.

Based on our study, we concluded that TDP-43 is a new rhythmic protein that regulates the expression of multiple circadian genes and affects circadian behavior by inhibiting *USP13* mRNA splicing. This affects the protein level of USP13 and ubiquitin-mediated degradation of BMAL1 and regulates the AMPK signaling pathway, glucose metabolism, and ATP production (Fig. 8 D).

Discussion

A bidirectional regulatory relationship exists between neurodegenerative diseases and circadian rhythm disorders. Rhythm disorders and sleep disturbances have become the main symptoms of most neurodegenerative diseases. Meanwhile, circadian rhythms and sleep disturbances may contribute to drive pathology in the early stages of neurodegenerative diseases. TDP-43 dysfunction or its pathological accumulation is associated with neurodegenerative diseases, such as ALS. This mainly affects motor neuron function in the brain and spinal cord. Therefore, we evaluated whether TDP-43 affects the circadian rhythm and contributes to the development of neurodegenerative diseases.

We propose that TDP-43 is a new member that participates in maintaining rhythm homeostasis. TDP-43 was expressed in a 24-h periodic oscillation in the hypothalamus, hippocampus, cortex, and liver of the mice, with a pattern similar to that of BMAL1 being different from in the cortex (Fig. 1). SD affected the oscillatory pattern of TDP-43 expression in the brain (Fig. S1, C and D), supporting a potential link between TDP-43 and sleep functions (Perlegos et al., 2024). TDP-43 regulated the expression of circadian rhythm-related genes in vitro and in vivo (Fig. 2, Fig. 3, and Fig. S2 A). The expression of BMAL1, CLOCK, and CRY1 proteins was restored in TDP-43-depleted cells by the ectopic expression of TDP-43 (Fig. S2 B). These results led us to deduce that TDP-43 is a component of the rhythm maintenance system, and that cellular TDP-43, at least in part, controls the function of multiple rhythm proteins. There may be bidirectional regulation between circadian homeostasis and TDP-43 function. Knockdown of TDP-43 mainly affected mRNA expression of multiple genes related to neurodegenerative diseases, such as ALS and AD, in our bulk RNA-seq analysis (Fig. 2, A and B). This is consistent with previous reports (Chen and Mitchell, 2021; Prater et al., 2022; Riku et al., 2022). These results also shed light on TDP-43 dysfunction by affecting rhythmic homeostasis, contributing to the development of neurodegenerative diseases.

We obtained data supporting a regulatory relationship between BMAL1 and TDP-43. Although BMAL1 was not found to have a role in controlling the circadian rhythm of the body (Koronowski et al., 2019), it is still believed to be a key molecular clock. *BMAL1* knockdown leads to the downregulation of other rhythm genes (Partch et al., 2014; Ray et al., 2020). *BMAL1* knockdown did not change the protein expression of TDP-43

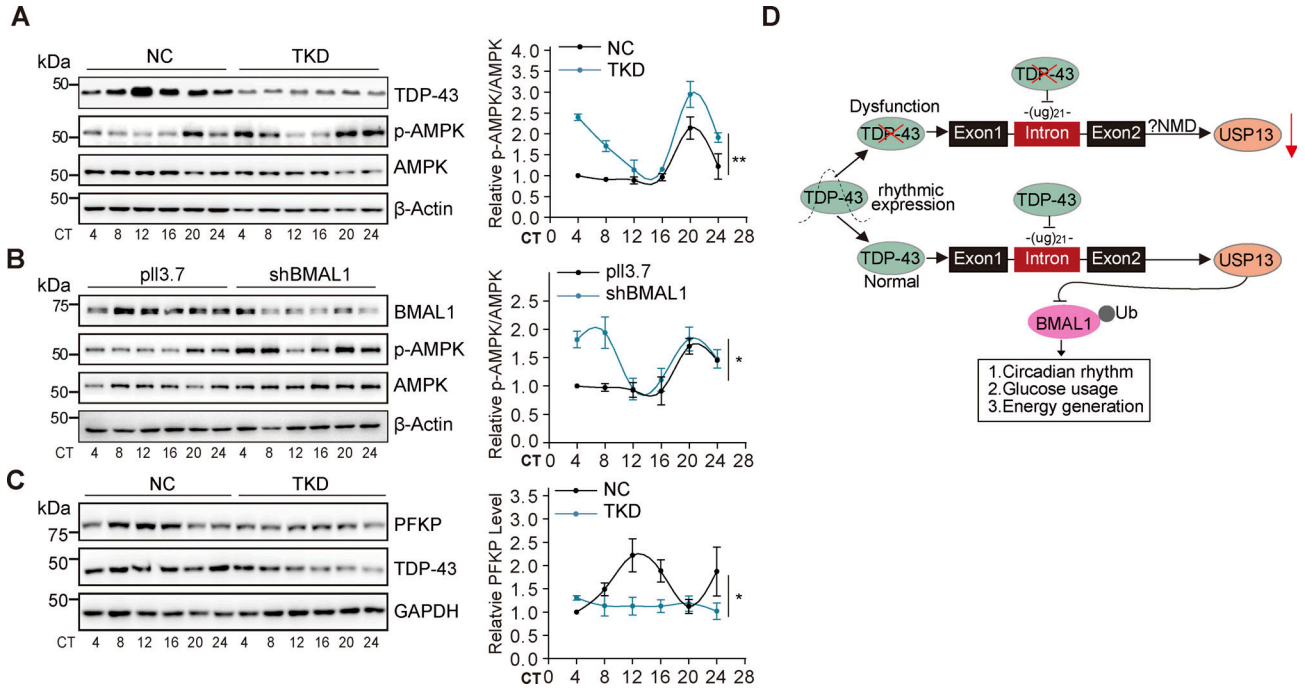

Figure 8. **TDP-43 and BMAL1 regulate the rhythmic expression of activated AMPK and PFKP. (A and B)** HEK-293T cells were transfected with PX458/TDP-43$_{KO}$ (TKD) (A), or pLL3.7/shBMAL1 (B) for 48 h. The cell lysates were analyzed using western blotting with indicated antibodies and quantitated (n = 3). **(C)** M17 cells were transfected with PX458/TKD for 48 h and then collected every 4 h over 24 h. The cell lysates were analyzed using western blotting with anti-PFKP and quantitated. **(D)** The proposed mechanism for TDP-43 affected circadian rhythm, glucose uptake, and energy generation. TDP-43 inhibited *USP13* intron 1 splicing, and its dysfunction downregulated USP13 expression and promoted ubiquitin-mediated degradation of BMAL1, through which circadian rhythm, glucose uptake, and ATP production were regulated. Data are presented as mean ± S.D. (n = 3) and compared with two-way RM ANOVA. *P < 0.05; **P < 0.01. Source data are available for this figure: SourceData F8.

(Fig. S2 C) and its knockout also did not change the rhythmic expression of TDP-43 (Fig. 7). However, overexpression of TDP-43 in *BMAL1* knockdown cells restored CLOCK, BMAL1, PER2, and CRY1 expression (Fig. S2 C). Because *Bmal1* knockout mice still exhibit a diurnal pattern of locomotion and feeding activity (Ray et al., 2020), and the rhythmic expression of TDP-43 was not influenced by the absence of *Bmal1*, we would deduce that the cyclic nature of TDP-43 expression is driven by rest–activity rhythms (RAR) (Innominato et al., 2023), either directly or indirectly, rather than by the circadian clock.

We identified the mechanism through which TDP-43 regulates BMAL1 signaling. The ubiquitin pathway plays a central role in regulating the circadian clock (Stojkovic et al., 2014). The ubiquitin–proteasome pathway was regulated by TDP-43 in transcriptomics (Fig. 2 A), and TDP-43 knockout promoted the ubiquitination of BMAL1 (Fig. 4, C and D). RNA-seq showed that TDP-43 regulated the mRNA and protein expression of USP13 (Fig. 2 A; and Fig. 5, B and C), and ectopic expression of TDP-43 restored the expression of USP13 (Fig. 5 B). *USP13* regulated ubiquitin modification and the protein level of BMAL1 (Fig. 5 G and Fig. 6). Its knockdown increased *USP13* intron 1 being spliced into *USP13* mRNA (Fig. 5 D), which decreased the amount of normal USP13 protein and attenuated the deubiquitination of BMAL1. Therefore, TDP-43 may inhibit *USP13* intron splicing by binding to the UG-rich RNA of *USP13* (Lukavsky et al., 2013). These findings have improved our understanding of the posttranslational regulation of BMAL1 protein (Fig. 8 D) and facilitated the investigation of the role of TDP-43 in modulating physiological and pathological functions through its impact on RNA processing (Tollervey et al., 2011).

We showed that the TDP-43–BMAL1 axis regulated cellular glucose use and energy production (Fig. S4). TDP-43 regulates the expression of glucose transporter genes, including GLUT2 and GLUT3, resulting in an altered glucose uptake (Fig. S4 D); this phenomenon was also endorsed in neurons (Manzo et al., 2019). PFKP, one of the key enzymes involved in glycolysis, was also identified as being regulated by TDP-43 and BMAL1 (Fig. 8 C; and Fig S5, A and B). TDP-43 knockdown led to a lower protein level of BMAL1 in cells under high glucose conditions (Fig. S4 E). This suggests that cellular rhythms may be more unstable in a hyperglycemic environment. Our findings indicate that circadian rhythms regulate glucose metabolism within organisms. We deduced that this regulation may be universally present in various organisms (Dyar et al., 2013; Marcheva et al., 2010). TDP-43 and BMAL1 also regulated the signal transduction of the energy sensor AMPK (Fig. 8, A and B). BMAL1 knockdown could induce energy stress by activating AMPK in cells (Lin and Hardie, 2018). This elucidates the mechanism by which the TDP-43–BMAL1 axis regulates cellular glucose usage to generate energy.

We found that TDP-43 regulated mammalian memory and balance in mice (Fig. 3, D and E), which is consistent with previous reports (Ma et al., 2021). Because icv-injected AAV carrying TDP-43 shRNA could circulate to the entire brain, TDP-43

knockdown was not limited to the hypothalamus. Therefore, we could not exclude the possibility that TDP-43 knockdown affected circadian behavior and that memory and balance abilities were induced by TDP-43 knockdown in other brain regions.

Based on these findings, we conclude that TDP-43, which is identified as a new rhythmic protein, regulates the expression of multiple circadian genes and affects circadian behavior, and cognitive and balance abilities in mice. TDP-43 may be an upstream regulator of BMAL1 because BMAL1 knockout did not change the rhythmic expression of TDP-43. We also propose that TDP-43 regulates the expression and alternative splicing of *USP13*, thereby affecting the protein level of USP13 and the ubiquitin-mediated degradation of BMAL1 and regulating the AMPK signaling pathway. This may result in changes in cellular glucose usage and ATP production. Our findings have enriched our understanding of the role of TDP-43 dysfunction in CRD in neurodegenerative diseases and provided new evidence supporting the interaction between CRD and neurodegeneration. Further, in-depth research will help to better understand more specific functions and finer regulatory signals in the rhythm function regulation of TDP-43.

Materials and methods

Animals

C57BL/6 mice were purchased from Wuxi AppTec. The *Bmal1*-floxed strain (JAX007668) was from Jackson Laboratory and was bred with EIIa-cre (JAX003724) to achieve whole body heterozygous *Bmal1*-deletion. The heterozygous *Bmal1*-deleted mouse line was then back-crossed to C57BL/6 for five generations prior to the standard heterozygote × heterozygote breeding for whole body *Bmal1*-knockout mice. All the mice were maintained at Nantong University Animal Colony. Mice were raised at temperatures of 21–22°C and subjected to a fixed light–day (12 h light/12 h dark) cycle with access to food and water ad libitum. Neonatal (P0) FVB mice used for fibroblast culture were bred in the Nantong University Animal Colony. All the animal experiments followed the ethical guidelines for animal research at the Nantong University (S20210302-032).

Cell culture and transfection

HEK-293T cells were cultured in Dulbecco's modified Eagle's medium (DMEM) supplemented with 10% fetal bovine serum (FBS) (Invitrogen). Human neuroblastoma M17 cells were cultured in DMEM/F12, also supplemented with 10% FBS. All the transfections were performed with Lipofectamine 2000 (Thermo Fisher Scientific) or jetPRIME (Polyplus Transfection) according to the manufacturer's instructions. For primary mouse brain fibroblast (MBF) culture, the cerebral meninges of fetal FVB mice (P0) were peeled off and placed in a Petri dish with precooled phosphate-buffered saline (PBS). Cerebral meninges were then cut into pieces followed by digestion with 0.25% trypsin at 37°C for 20 min and preparation of a cell suspension. Following filtration, the cells were collected by centrifugation before being resuspended in DMEM containing 10% FBS, 100 U/ml penicillin, and 100 µg/ml streptomycin. The cells were adjusted to ~8×10^4/ml and maintained in a 3.5 cm Petri dish at 37°C with 5% CO_2.

Plasmids and viruses

pCI/TDP-43 tagged with hemagglutinin (HA) was constructed by our group (Gu et al., 2017a). pcDNA3.1/Flag-BMAL1 and pcDNA3.1/His-USP13 were provided by Dr. Xu of Soochow University and Dr. Sun of Wuhan University, respectively (Sun et al., 2017; Ullah et al., 2020). pAdeno-associated virus (AAV) serotype2/9-CBG-enhanced green fluorescent protein (EGFP)-3×FLAG-WPRE-H1-shRNA targeting TARDBP, pSLenti-U6-shRNA (TARDBP)-CMV-EGFP-F2A-Puro-WPRE (mouse), and their corresponding control viruses were constructed and packaged by OBiO Technology Co., Ltd. Using pcDNA3.1/His-USP13 as a template, PCR amplification was used to obtain the USP13 coding sequence carrying *Xho*I and *Not*I clone site; the resulting PCR fragment was cut with two enzymes and was then inserted into the pGEX-4T-1 vector between the sites, obtaining pGEX-4T-USP13. To generate His-BMAL1, BMAL1 cDNA was produced by PCR with full-length cDNA BMAL1 as a template. The resulting BMAL1 PCR fragment was inserted into the pET-30a vector between *Bgl*II and *Not*I sites, obtaining pGEX-4T-BMAL1. pGEX-4T-USP13 and pGEX-4T-BMAL1 were used for producing recombinant GST fusion USP13 and BMAL1. For pcDNA3.1/USP13-C345A construction, the mutant USP13 coding sequence was amplified by PCR using the following primer pairs: 5′-GACAGAGCTGAGATAGGCGCTGTTGCCCAGGTTC-3′ and 5′-GAACCTGGGCAACAGCGCCTATCTCAGCTCTGTC-3′, and be cloned into pcDNA3.1 vector. LentiCRISPR v2/TDP-43_{KO} and pSpCas9(BB)-2A-GFP (PX458)/TDP-43_{KO} (TKD) were constructed by clustered regularly interspaced short palindromic repeat–associated endonuclease Cas9 (CRISPR-CAS9), and the gDNA sequence was 5′-GGTTACAGCCCAGTTTCCAG-3′. The lentiviruses shTDP-43, shBMAL1, and shUSP13 were constructed by inserting interfering sequences into pLL3.7 (Addgene). The target sequences for shRNAs were TDP-43_1 (human): 5′-GCA GGTCAAGAAAGATCTTAA-3′, TDP-43_2 (human): 5′-AGATCT TAAGACTGGTCATTC-3′, TDP-43 (mouse): 5′- GCAAACTTCCTA ATTCTAAGC-3′, BMAL1 (human): 5′-CTTCTAGGCACATCGTGT TAT-3′, and USP13 (human): 5′-CGCCTGATGAACCAATTGATA-3′.

Antibodies and reagents

Primary antibodies used in this study are listed in Table S1. 2-(n-7-nitro-2,1, 3-benzoxadiazole-4-amino)-2-deoxy-glucose (NBDG) glucose uptake assay kit was purchased from Invitrogen. Protein G beads, ECL western blotting substrates, Alexa 555-conjugated goat anti-mouse IgG, Alexa 488-conjugated goat anti-rabbit IgG, and Cy3-conjugated goat anti-rabbit IgG were purchased from Thermo Fisher Scientific. Horseradish peroxidase (HRP)-conjugated anti-mouse and anti-rabbit IgG antibodies were from Jackson ImmunoResearch Laboratories. MG-132 (Z-Leu-Leu-Leu-al) and CHX (CHX) was from MedChemExpress LLC.

Stereotaxic intracerebroventricular injection

8-wk-old C57BL/6 mice were intraperitoneally anesthetized with a 1.25% solution of 2,2,2-tribromoethanol (Sigma-Aldrich). After hair removal, a sagittal scalp incision was made and a burr hole was drilled in the skull. Stereotaxic injection of 1 µl of AAV

viruses was performed bilaterally into the intracerebroventricular (icv) region using coordinates of 0.5 mm A/P and ±1.0 mm M/liter relative to the bregma and 2.5 mm beneath the skull surface. The viruses were injected at a rate of 0.4 µl/min using a Hamilton syringe equipped with a 31-gauge cemented needle, which was automated using an injection pump. The needle was left in place for 5 min before slow withdrawal. The skin incision was closed using a surgical staple. During and after surgery, the animals were kept warm on a heating pad until they fully recovered from the anesthesia. The survival of the animals was monitored daily. 1 mo after the injection, the mice underwent synchronization treatment for 1 wk and were then subjected to behavioral assays. Subsequently, the mice were sacrificed and their brains were collected for further experiments.

Sleep deprivation

8-wk-old C57BL/6 mice were synchronized for 4 wk and randomly assigned to two groups without blinding. SD was performed at four zeitgeist times of the day, that is, ZT0, ZT6, ZT12, and ZT18, This was conducted using an SD instrument (Sansbio) (Curie et al., 2015), in which the animals were kept in a cage with a motor system controlling a sweeper bar at torque, speed, and operating frequency. After 5.5 h of SD, the treated or non-sleep-deprived control mice were sacrificed in 30 min, and the brain and liver were collected and stored at −80°C.

Locomotor activity

1 mo after the AAV virus injection, the mice were raised in a cage with a running wheel and an independent ventilation system for 3 wk in a 12-h light/12-h dark (LD) sequence. This was followed by a continuous dark (DD) status for another 3 wk. To examine the phase shift in locomotor activity, a wireless running wheel system (80820s; Campden) carrying a sensor hub was used to measure the wheel-running activity of the mice and circadian phase differences, according to the manufacturer's instructions. Actograms and chi-square periodograms were analyzed and generated using ClockLab Analysis 6 software (Actimetric).

Open field test, rotarod test, and Morris water maze

Open field and Morris water maze (MWM) experiments were performed using a video monitoring system (ANYmaze; Stoelting Co.) for recording and analysis. In the open field test, the mice were set in a black plastic arena ("L × W × H" is 48 cm × 48 cm × 40 cm) and recorded every 150 s over four sequential sessions. A square area of 225 cm^3 in the central region of the open field was designated as the central zone. The cumulative distance traveled, duration of immobility, average speed, time spent within the central zone, frequency of entry into the central zone, and average distance from the central zone were recorded for each animal.

During the rotarod test, mice were subjected to three trials per day for five consecutive days using a rotarod apparatus (Ugo Basile). The rotarod gradually increased its speed from four revolutions per minute (rpm) to 40 rpm within a span of 2 min. Each trial had a maximum duration of 500 s and the mice were given a 30-min rest period between each trial.

For the MWM test, mice were placed in a black circular pool and separated into four equal quadrants. In each quadrant, a submerged escape platform, measuring 13 cm in diameter, was positioned 1 cm below the water surface. During each training trial, mice were allowed a maximum of 90 s to explore the maze freely. If the mouse failed to reach the platform within the allocated time, it was gently guided to the platform. After each trial, the mouse remained on the platform for 20 s. This training routine was repeated four times per day for four consecutive days, with a break of >30 min between each trial. 24 h after the final training session, a probe trial was conducted for 90 s without an escape platform. Spatial memory was assessed by measuring the time taken to reach the platform zone, swimming speed, and distance traveled until the mouse first reached the target zone.

Cycloheximide and MG132 treatment

For the CHX (MCE) treatment, M17 cells were transfected with PX458/TDP-43_{KO} (TKD). 48 h later, the cells were synchronized by being cultured in DMEM/50% horse serum for 2 h and then DMEM/1% FBS for 22 h. Thereafter, the cells were treated with 200 µg/ml CHX at CT8, and the cell lysates were extracted every 4 h. For the proteasome inhibition experiments, M17 cells were infected with Lenti/shTDP-43. After a 24 h period, the cells were synchronized and exposed to 10 µM MG132 (MCE) for a duration of 12 h. Following this treatment, the cells were harvested at CT12 and their lysates were used for western blot analysis.

Immunofluorescence staining

Cells were seeded onto glass coverslips in 24-well plates one day prior to transfection, reaching ∼30% confluence. Cells were fixed with 4% paraformaldehyde in PBS for 30 min at 25°C. After PBS washing, the cells were blocked for 2 h at 37°C in 10% goat serum diluted in PBS containing 0.2% Triton X-100. The cells were incubated overnight at 4°C with monoclonal anti-BMAL1 (1:500), anti-CLOCK (1:500), polyclonal anti-PER2 (1:500), or anti-CRY1 (1:500) antibodies. After washing, the cells were incubated at 25°C for 2 h with Alexa 488-conjugated goat anti-rabbit IgG or Alexa 555-conjugated goat anti-mouse IgG, both at a dilution of 1:500, along with Hoechst dye at 1:5,000 dilution for nuclear staining. Following a PBS wash, the cells were mounted using ProLong Gold antifade reagent (Thermo Fisher Scientific) and observed using a Leica TCS-SP2 laser scanning confocal microscope.

For the staining of a mouse brain, adult C57BL/6 mice were anesthetized and fixed by cardiac infusion with 4% PFA at ZT0, ZT4, ZT8, ZT12, ZT16, and ZT20, and then frozen sections were performed after gradient dehydration with sucrose. Free-floating sections, 40 µm in thickness, of the cortex were washed with three changes of PBS, subsequently subjected to blocking with 10% goat serum in 0.5% Triton X-100/PBS for 2 h at 37°C after permeabilization, and then incubated with polyclonal anti-TDP-43 (Proteintech, 1:1,000) overnight at 4°C. Then, they were washed with PBS and incubated for 2 h with Cy3-conjugated goat anti-rabbit IgG (Thermo Fisher Scientific, 1:400) at room temperature. After washing with PBS, the sections were mounted with DAPI Fluoromount-G (SouthernBiotech; Amersco), and observed with OLYMPUS FV300 laser scanning confocal microscope.

GST pull down assay

GST and His-fusion proteins were purified as described (Zhang et al., 2014). Briefly, BL21 cells harboring the GST or various GST and His recombinant expression plasmids were grown to log phase and induced with 0.1 mM IPTG for 2 h at 37°C. Bacteria were collected and resuspended in lysis buffer and sonicated. Solubilized proteins were recovered by centrifugation and incubated with glutathione-agarose beads or Ni-NTA beads for 4 h at 4°C and washed several times with ice-cold PBS. The resulting bead-bound proteins were eluted with an elution buffer. Then, the eluted proteins were subjected to dialysis against PBS overnight at 4°C.

For in vitro binding assays, GST-USP13 or GST was mixed with His-BMAL1 in a GST pull-down buffer (20 mM Tris-HCl, pH 7.5, 150 mM NaCl, 0.1% Triton X-100, 1 mM DTT, 10% glycerol) at 4°C overnight. Then glutathione sepharose was added and samples were rotated at 4°C for 1 h. After washing three times, the bound proteins were separated on SDS-PAGE followed by western blotting analysis.

Immunoprecipitation (IP) and co-immunoprecipitation (co-IP)

For IP, the cells or mice brains were lysed in a lysis buffer containing 50 mM Tris-HCl (pH 7.4), 150 mM NaCl, 0.2% NaDox, 0.1% NP-40, 0.1% Triton X-100, 1 mM Na_3VO_4, 50 mM NaF, 2 mM EDTA, and protease inhibitor cocktail (1:1,000). For co-IP, the cells were lysed using sonication in lysis buffer containing 50 mM Tris-HCl (pH 7.4), 150 mM NaCl, 1 mM Na_3VO_4, 50 mM NaF, 2 mM EDTA, and cocktail (1:1,000). The extract was then centrifuged at 15,000*g*, for 5 min at 4°C. The resulting lysate was incubated overnight at 4°C with protein G beads precoupled with monoclonal antibodies. The beads were washed twice with lysis buffer and Tris-buffered saline (TBS). The bound proteins were eluted by boiling in 2× Laemmli sample buffer and subjected to western blotting analysis.

RNA sequencing (RNA-seq)

M17 cells were infected with viruses engineered to deliver guide RNA (gRNA) targeting the *TARDBP* gene (see LentiCRISPR v2/TDP-43_{KO} in "Plasmids and viruses" section) or control viruses, synchronized for 36 h, and then collected with TRIzol reagent at CT12. The samples were sent to Huada Gene Company for digital gene expression analysis. For sequencing, Illumina technology was used with minor adjustments, resulting in millions of raw reads generated in each sequencing tunnel with a sequencing length of 49 bp. Quality evaluation of the RNA-seq data was conducted by analyzing the tag distribution of each group. To functionally annotate the differentially expressed genes, the Huada Gene Company performed gene ontology (GO) annotation and KEGG pathway analyses. The raw data of the RNA-seq was uploaded to gene expression omnibus (GEO) database (GSE260737).

Western blotting

10% homogenate of mouse tissue was prepared in a buffer containing 20 mM Tris-HCl (pH 8.0), 0.32 M sucrose, 10 mM β-ME, 5 mM $MgSO_4$, 1 mM EDTA, 1 mM Na_3VO_4, and 50 mM NaF, along with a cocktail of protease inhibitors (diluted 1:1,000). The homogenate was then centrifuged at 15,000*g* for 30 min at 4°C. The resulting extract and cells were lysed in 1× Laemmli buffer and boiled for 5 min in a thermostatic metal bath (JOANLAB). The samples were resolved using 10% SDS-PAGE and transferred onto an Immobilon-P transfer membrane (Merck Millipore). The blots were incubated overnight with primary antibodies, followed by incubation with the corresponding horseradish peroxidase-conjugated secondary antibodies at room temperature for 2 h. The blots were developed using Pierce ECL Western Blotting Substrate (Thermo Fisher Scientific) and visualized using a Tanon-5200 Chemiluminescence imager (Biotanon Ltd.). The specific immunosignal was quantified using Multi Gauge software (V3.0; Fuji Film).

RNA isolation, reverse transcription PCR (RT-PCR), and quantitative real-time PCR (RT-qPCR)

Total RNA was isolated from cells or tissues using the RNA isolator Total RNA Extraction Reagent (Vazyme) and then reverse-transcribed using BL699A reverse transcription kit (Biosharp). The RNA splicing of USP13 was measured by PCR (Vazyme) with forward primer 5′-ACGAGAAGGGAAGCAGAAGC-3′ and reverse primer 5′-TTGGTTCATCAGGCGATCTT-3′. The PCR products were resolved on 1.5% agarose gels, visualized by gel red staining, and quantitated using the Molecular Imager system (Bio-Rad).

The qPCR reactions were performed using AceQ qPCR SYBR Green Master Mix (Vazyme) with LightCycler 96 Real-Time PCR System (Roche Diagnostics) according to the manufacturer's instructions. The primers used for qPCR are listed in Table S2. All the reactions were performed in triplicate. The qPCR reactions were conducted as follows: 3 min at 95°C for the initial denaturation, followed by 45 cycles of amplification at 95°C for 10 s and 60°C for 15 s, and then 95°C for 10 s, 65°C for 1 min, and 97°C for 1 s. The $2^{-\Delta\Delta CT}$ method, with GAPDH as the internal control, was used to determine the relative expression.

Chromatin immunoprecipitation

M17 cells cultured on 10-cm plates at 90% confluence were treated with formaldehyde added to the culture medium at a final concentration of 1% (vol/vol). The reaction was maintained at 25°C with shaking for 10 min, after which glycine (0.125 M) was added. After 10 min, the cells were rinsed twice with cold PBS supplemented with 1 mM phenylmethylsulfonyl fluoride (PMSF). The cells were harvested and lysed in SDS lysis buffer containing 1 mM PMSF, 2 mg/ml pepstatin A, and 2 mg/ml aprotinin. DNA was fragmented into 400–1,100 bp fragments using sonication. The chromatin was precleared and incubated overnight at 4°C with agarose beads coupled with either control antiserum or anti-BMAL1 (Abcam).

The agarose beads were collected by centrifugation and washed sequentially with low-salt, high-salt, LiCl, and TE buffers (twice each). After reversing the protein/DNA cross-links, DNA was isolated using phenol/chloroform extraction and ethanol precipitation and used as a template for standard PCR amplification. The PCR products were separated on a 2.0% agarose gel and stained with ethidium bromide. The resulting samples were visualized under UV light and the PCR products were purified and sequenced.

Determination of cellular TCA metabolism intermediates and energy metabolites using mass spectrometry

Cellular TCA metabolism intermediates and energy metabolites were detected using mass spectrometry with multiple reaction monitoring (MRM) techniques. Briefly, M17 cells infected with viruses engineered to deliver gRNA targeting the *TARDBP* gene (see LentiCRISPR v2/TDP-43_{KO} in "Plasmid and virus" section) or control viruses for 72 h. After synchronization for 36 h, the cells in each group were washed with PBS three times, scraped, and centrifuged at 1,000*g* for 5 min. More than 10 million cells were rapidly frozen in liquid nitrogen and metabolic analyses were performed (Shanghai Applied Protein Technology).

Glucose uptake assay

M17 cells in the 24-well plates were transfected with the TDP-43 gene editor vector, and after 48 h, the medium was changed to sugar-free DMEM with 200 μM 2-NBDG (Invitrogen) for 30 min. The cells were washed three times with PBS for 3 min, the green fluorescence of the cells was observed, and images were captured under a microscope. The fluorescence intensity of 2-NBDG was measured using a luminometer. Liver homogenates from AAV tail vein-injected mice were subjected to a glucose assay kit with O-toluidine (Beyotime Biotechnology) to measure the concentration of the glucose (μg/mg protein) according to the manufacturer's instructions.

Statistical analysis

The data are presented as the mean ± S.D. (Standard Deviation), and GraphPad Prism 8 (GraphPad Software Inc.) was used for statistical analysis. The results were analyzed using one-way ANOVA, unpaired *t* test, two-way RM ANOVA, or *JTK*_Cycle analysis. A value of $P < 0.05$ was considered statistically significant.

Online supplemental material

Fig. S1 shows the representative area of the suprachiasmatic nucleus (SCN) where used to quantify and the quantification results for Fig. 1 C, along with the observation that sleep deprivation alters the rhythmic expression of TDP-43 in the hypothalamus of mice. Fig. S2 shows that TDP-43 regulates the expression of BMAL1, CLOCK, PER2, and CRY1 in cultured cells. Fig. S3 shows that USP13 exhibits rhythmic oscillations in expression in M17 cells. Fig. S4 shows that TDP43 regulates cellular glucose uptake, glycolysis, TCA cycle, and energy production. Fig. S5 shows TDP-43 controlled neuronal glycolysis possibly by directly regulating the transcription of PFKP through BMAL1. Table S1 affords the information of primary antibodies used in this study. Table S2 shows the primers used for qPCR and ChIP in this study. Data S1 shows all source files for immunoblot experiments in excel file. Data S2 shows all source files for immunoblot experiments in PDF file.

Data availability

Further information and requests for resources and reagents should be directed to and will be fulfilled by the lead contact, H. Cui (hengxiangc@qq.com).

Acknowledgments

We are grateful to Drs. Hung-Chun Chang, Shujia Zhu, and Tingyu Shen (Shanghai Center for Brain Science and Brain-inspired Technology, Shanghai, China) for providing *Bmal1* knockout mice and assistance during the wheel-running experiment. We would like to thank Editage (https://www.editage.cn) for English language editing.

This study was supported by the National Natural Science Foundation of China (32171258, 31870772), the Natural Science Foundation of Jiangsu Province (BK20211329), and funds from the Co-Innovation Center of Neuroregeneration and the NMPA Key Laboratory for Research and Evaluation of Tissue Engineering Technology Products of Nantong University.

Author contributions: J. Gu: Conceptualization, Data curation, Formal analysis, Funding acquisition, Investigation, Methodology, Project administration, Resources, Supervision, Validation, Visualization, Writing - original draft, Writing - review & editing, M. Yang: Investigation, L. Zhang: Investigation, Validation, Visualization, Y. Liu: Data curation, Software, R. Yan: Investigation, D. Pan: Validation, X. Qian: Project administration, Validation, H. Hu: Methodology, D. Chu: Resources, C. Hu: Conceptualization, Investigation, Methodology, Project administration, Resources, Validation, Writing - review & editing, F. Liu: Conceptualization, Supervision, Visualization, Writing - review & editing, H. Cui: Conceptualization, Data curation, Formal analysis, Funding acquisition, Investigation, Methodology, Project administration, Resources, Software, Supervision, Validation, Visualization, Writing - original draft, Writing - review & editing.

Disclosures: The authors declare no competing interests exist.

Submitted: 24 May 2024
Revised: 20 November 2024
Accepted: 11 February 2025

References

Bolsius, Y.G., M.D. Zurbriggen, J.K. Kim, M.J. Kas, P. Meerlo, S.J. Aton, and R. Havekes. 2021. The role of clock genes in sleep, stress and memory. *Biochem. Pharmacol.* 191:114493. https://doi.org/10.1016/j.bcp.2021.114493

Chen, H.J., and J.C. Mitchell. 2021. Mechanisms of TDP-43 proteinopathy onset and propagation. *Int. J. Mol. Sci.* 22:6004. https://doi.org/10.3390/ijms22116004

Chen, J., L. Zou, G. Lu, O. Grinchuk, L. Fang, D.S.T. Ong, R. Taneja, C.N. Ong, and H.M. Shen. 2022. PFKP alleviates glucose starvation-induced metabolic stress in lung cancer cells via AMPK-ACC2 dependent fatty acid oxidation. *Cell Discov.* 8:52. https://doi.org/10.1038/s41421-022-00406-1

Corbet, G.A., J.R. Wheeler, R. Parker, and K. Weskamp. 2021. TDP43 ribonucleoprotein granules: Physiologic function to pathologic aggregates. *RNA Biol.* 18:128–138. https://doi.org/10.1080/15476286.2021.1963099

Curie, T., S. Maret, Y. Emmenegger, and P. Franken. 2015. In vivo imaging of the central and peripheral effects of sleep deprivation and suprachiasmatic nuclei lesion on PERIOD-2 protein in mice. *Sleep.* 38:1381–1394. https://doi.org/10.5665/sleep.4974

Dyar, K.A., S. Ciciliot, L.E. Wright, R.S. Biensø, G.M. Tagliazucchi, V.R. Patel, M. Forcato, M.I. Paz, A. Gudiksen, F. Solagna, et al. 2013. Muscle insulin sensitivity and glucose metabolism are controlled by the intrinsic muscle clock. *Mol. Metab.* 3:29–41. https://doi.org/10.1016/j.molmet.2013.10.005

Fang, Xiaoguang, Wenchao Zhou, Qiulian Wu, Zhi Huang, Yu Shi, Kailin Yang, Cong Chen, Qi Xie, Stephen C Mack, Xiuxing Wang, et al. 2017. Deubiquitinase USP13 maintains glioblastoma stem cells by antagonizing FBXL14-mediated Myc ubiquitination. *J Exp Med*. 214:245–267. https://doi.org/10.1084/jem.20151673

Flores, B.N., X. Li, A.M. Malik, J. Martinez, A.A. Beg, and S.J. Barmada. 2019. An intramolecular salt bridge linking TDP43 RNA binding, protein stability, and TDP43-dependent neurodegeneration. *Cell Rep.* 27: 1133–1150.e8. https://doi.org/10.1016/j.celrep.2019.03.093

Gu, J., F. Chen, K. Iqbal, C.X. Gong, X. Wang, and F. Liu. 2017a. Transactive response DNA-binding protein 43 (TDP-43) regulates alternative splicing of tau exon 10: Implications for the pathogenesis of tauopathies. *J. Biol. Chem.* 292:10600–10612. https://doi.org/10.1074/jbc.M117.783498

Gu, J., F. Wu, W. Xu, J. Shi, W. Hu, N. Jin, W. Qian, X. Wang, K. Iqbal, C.X. Gong, and F. Liu. 2017b. TDP-43 suppresses tau expression via promoting its mRNA instability. *Nucleic Acids Res.* 45:6177–6193. https://doi.org/10.1093/nar/gkx175

Hirano, A., T. Nakagawa, H. Yoshitane, M. Oyama, H. Kozuka-Hata, D. Lanjakornsiripan, and Y. Fukada. 2016. USP7 and TDP-43: Pleiotropic regulation of cryptochrome protein stability paces the oscillation of the mammalian circadian clock. *PLoS One*. 11:e0154263. https://doi.org/10.1371/journal.pone.0154263

Innominato, P.F., N.I. Wreglesworth, A. Karaboué, D. Spiegel, and F.A. Lévi. 2023. Rest-activity rhythm as a clinical biomarker in cancer. *Lancet Healthy Longev*. 4:e304. https://doi.org/10.1016/S2666-7568(23)00108-3

Jiang, X., T. Zhang, H. Wang, T. Wang, M. Qin, P. Bao, R. Wang, Y. Liu, H.C. Chang, J. Yan, and J. Xu. 2018. Neurodegeneration-associated FUS is a novel regulator of circadian gene expression. *Transl. Neurodegener*. 7:24. https://doi.org/10.1186/s40035-018-0131-y

Josephs, K.A., J.L. Whitwell, S.D. Weigand, M.E. Murray, N. Tosakulwong, A.M. Liesinger, L. Petrucelli, M.L. Senjem, D.S. Knopman, B.F. Boeve, et al. 2014. TDP-43 is a key player in the clinical features associated with Alzheimer's disease. *Acta Neuropathol.* 127:811–824. https://doi.org/10.1007/s00401-014-1269-z

Koronowski, K.B., K. Kinouchi, P.S. Welz, J.G. Smith, V.M. Zinna, J. Shi, M. Samad, S. Chen, C.N. Magnan, J.M. Kinchen, et al. 2019. Defining the independence of the liver circadian clock. *Cell*. 177:1448–1462.e14. https://doi.org/10.1016/j.cell.2019.04.025

Lamia, K.A., U.M. Sachdeva, L. DiTacchio, E.C. Williams, J.G. Alvarez, D.F. Egan, D.S. Vasquez, H. Juguilon, S. Panda, R.J. Shaw, et al. 2009. AMPK regulates the circadian clock by cryptochrome phosphorylation and degradation. *Science*. 326:437–440. https://doi.org/10.1126/science.1172156

Lin, S.C., and D.G. Hardie. 2018. AMPK: Sensing glucose as well as cellular energy status. *Cell Metab.* 27:299–313. https://doi.org/10.1016/j.cmet.2017.10.009

Liu, X., R. Dai, M. Ke, I. Suheryani, W. Meng, and Y. Deng. 2017. Differential proteomic analysis of dimethylnitrosamine (DMN)-induced liver fibrosis. *Proteomics*. 17. https://doi.org/10.1002/pmic.201700267

Loganathan, S., B.A. Wilson, S.B. Carey, E. Manzo, A. Joardar, B. Ugur, and D.C. Zarnescu. 2022. TDP-43 proteinopathy causes broad metabolic alterations including TCA cycle intermediates and dopamine levels in Drosophila models of ALS. *Metabolites*. 12:101. https://doi.org/10.3390/metabo12020101

Lukavsky, P.J., D. Daujotyte, J.R. Tollervey, J. Ule, C. Stuani, E. Buratti, F.E. Baralle, F.F. Damberger, and F.H. Allain. 2013. Molecular basis of UG-rich RNA recognition by the human splicing factor TDP-43. *Nat. Struct. Mol. Biol.* 20:1443–1449. https://doi.org/10.1038/nsmb.2698

Ma, P., Y. Li, H. Wang, and B. Mao. 2021. Haploinsufficiency of the TDP43 ubiquitin E3 ligase RNF220 leads to ALS-like motor neuron defects in the mouse. *J. Mol. Cell Biol.* 13:374–382. https://doi.org/10.1093/jmcb/mjaa072

Maksimovic, K., M. Youssef, J. You, H.K. Sung, and J. Park. 2023. Evidence of metabolic dysfunction in amyotrophic lateral sclerosis (ALS) patients and animal models. *Biomolecules*. 13:863. https://doi.org/10.3390/biom13050863

Manzo, E., I. Lorenzini, D. Barrameda, A.G. O'Conner, J.M. Barrows, A. Starr, T. Kovalik, B.E. Rabichow, E.M. Lehmkuhl, D.D. Shreiner, et al. 2019. Glycolysis upregulation is neuroprotective as a compensatory mechanism in ALS. *Elife*. 8:e45114. https://doi.org/10.7554/eLife.45114

Marcheva, B., K.M. Ramsey, E.D. Buhr, Y. Kobayashi, H. Su, C.H. Ko, G. Ivanova, C. Omura, S. Mo, M.H. Vitaterna, et al. 2010. Disruption of the clock components CLOCK and BMAL1 leads to hypoinsulinaemia and diabetes. *Nature*. 466:627–631. https://doi.org/10.1038/nature09253

Marpegan, L., A.E. Swanstrom, K. Chung, T. Simon, P.G. Haydon, S.K. Khan, A.C. Liu, E.D. Herzog, and C. Beaulé. 2011. Circadian regulation of ATP release in astrocytes. *J. Neurosci.* 31:8342–8350. https://doi.org/10.1523/JNEUROSCI.6537-10.2011

McGoldrick, P., and J. Robertson. 2023. Unraveling the impact of disrupted nucleocytoplasmic transport systems in C9orf72-associated ALS. *Front. Cell. Neurosci.* 17:1247297. https://doi.org/10.3389/fncel.2023.1247297

Musiek, E.S., and D.M. Holtzman. 2016. Mechanisms linking circadian clocks, sleep, and neurodegeneration. *Science*. 354:1004–1008. https://doi.org/10.1126/science.aah4968

Nassan, M., and A. Videnovic. 2022. Circadian rhythms in neurodegenerative disorders. *Nat. Rev. Neurol.* 18:7–24. https://doi.org/10.1038/s41582-021-00577-7

Neumann, M., D.M. Sampathu, L.K. Kwong, A.C. Truax, M.C. Micsenyi, T.T. Chou, J. Bruce, T. Schuck, M. Grossman, C.M. Clark, et al. 2006. Ubiquitinated TDP-43 in frontotemporal lobar degeneration and amyotrophic lateral sclerosis. *Science*. 314:130–133. https://doi.org/10.1126/science.1134108

Partch, C.L., C.B. Green, and J.S. Takahashi. 2014. Molecular architecture of the mammalian circadian clock. *Trends Cell Biol.* 24:90–99. https://doi.org/10.1016/j.tcb.2013.07.002

Patke, A., M.W. Young, and S. Axelrod. 2020. Molecular mechanisms and physiological importance of circadian rhythms. *Nat. Rev. Mol. Cell Biol.* 21:67–84. https://doi.org/10.1038/s41580-019-0179-2

Peng, F., X. Li, F. Xiao, R. Zhao, and Z. Sun. 2022a. Circadian clock, diurnal glucose metabolic rhythm, and dawn phenomenon. *Trends Neurosci.* 45: 471–482. https://doi.org/10.1016/j.tins.2022.03.010

Peng, X., R. Fan, L. Xie, X. Shi, K. Dong, S. Zhang, J. Tao, W. Xu, D. Ma, J. Chen, and Y. Yang. 2022b. A growing link between circadian rhythms, type 2 diabetes mellitus and Alzheimer's disease. *Int. J. Mol. Sci.* 23:504. https://doi.org/10.3390/ijms23010504

Perlegos, A.E., J. Durkin, S.J. Belfer, A. Rodriguez, O. Shcherbakova, K. Park, J. Luong, N.M. Bonini, and M.S. Kayser. 2024. TDP-43 impairs sleep in Drosophila through Ataxin-2-dependent metabolic disturbance. *Sci. Adv.* 10:eadj4457. https://doi.org/10.1126/sciadv.adj4457

Polymenidou, M., C. Lagier-Tourenne, K.R. Hutt, S.C. Huelga, J. Moran, T.Y. Liang, S.C. Ling, E. Sun, E. Wancewicz, C. Mazur, et al. 2011. Long pre-mRNA depletion and RNA missplicing contribute to neuronal vulnerability from loss of TDP-43. *Nat. Neurosci.* 14:459–468. https://doi.org/10.1038/nn.2779

Prater, K.E., C.S. Latimer, and S. Jayadev. 2022. Glial TDP-43 and TDP-43 induced glial pathology, focus on neurodegenerative proteinopathy syndromes. *Glia*. 70:239–255. https://doi.org/10.1002/glia.24096

Ray, S., U.K. Valekunja, A. Stangherlin, S.A. Howell, A.P. Snijders, G. Damodaran, and A.B. Reddy. 2020. Circadian rhythms in the absence of the clock gene Bmal1. *Science*. 367:800–806. https://doi.org/10.1126/science.aaw7365

Richards, J., and M.L. Gumz. 2013. Mechanism of the circadian clock in physiology. *Am. J. Physiol. Regul. Integr. Comp. Physiol.* 304:R1053–R1064. https://doi.org/10.1152/ajpregu.00066.2013

Riku, Y., Y. Iwasaki, S. Ishigaki, A. Akagi, M. Hasegawa, K. Nishioka, Y. Li, M. Riku, T. Ikeuchi, Y. Fujioka, et al. 2022. Motor neuron TDP-43 proteinopathy in progressive supranuclear palsy and corticobasal degeneration. *Brain*. 145:2769–2784. https://doi.org/10.1093/brain/awac091

Roczniak-Ferguson, A., and S.M. Ferguson. 2019. Pleiotropic requirements for human TDP-43 in the regulation of cell and organelle homeostasis. *Life Sci. Alliance*. 2:e201900358. https://doi.org/10.26508/lsa.201900358

Ruan, W., X. Yuan, and H.K. Eltzschig. 2021. Circadian rhythm as a therapeutic target. *Nat. Rev. Drug Discov.* 20:287–307. https://doi.org/10.1038/s41573-020-00109-w

Schmitt, K., A. Grimm, R. Dallmann, B. Oettinghaus, L.M. Restelli, M. Witzig, N. Ishihara, K. Mihara, J.A. Ripperger, U. Albrecht, et al. 2018. Circadian control of DRP1 activity regulates mitochondrial dynamics and bioenergetics. *Cell Metab.* 27:657–666.e5. https://doi.org/10.1016/j.cmet.2018.01.011

Shrinivas, K., B.R. Sabari, E.L. Coffey, I.A. Klein, A. Boija, A.V. Zamudio, J. Schuijers, N.M. Hannett, P.A. Sharp, R.A. Young, and A.K. Chakraborty. 2019. Enhancer features that drive formation of transcriptional condensates. *Mol. Cell*. 75:549–561.e7. https://doi.org/10.1016/j.molcel.2019.07.009

Stojkovic, K., S.S. Wing, and N. Cermakian. 2014. A central role for ubiquitination within a circadian clock protein modification code. *Front. Mol. Neurosci.* 7:69. https://doi.org/10.3389/fnmol.2014.00069

Sun, H., Q. Zhang, Y.Y. Jing, M. Zhang, H.Y. Wang, Z. Cai, T. Liuyu, Z.D. Zhang, T.C. Xiong, Y. Wu, et al. 2017. USP13 negatively regulates antiviral responses by deubiquitinating STING. *Nat. Commun.* 8:15534. https://doi.org/10.1038/ncomms15534

Tollervey, J.R., T. Curk, B. Rogelj, M. Briese, M. Cereda, M. Kayikci, J. König, T. Hortobágyi, A.L. Nishimura, V. Zupunski, et al. 2011. Characterizing the RNA targets and position-dependent splicing regulation by TDP-43. *Nat. Neurosci.* 14:452–458. https://doi.org/10.1038/nn.2778

Ullah, K., S. Chen, J. Lu, X. Wang, Q. Liu, Y. Zhang, Y. Long, Z. Hu, and G. Xu. 2020. The E3 ubiquitin ligase STUB1 attenuates cell senescence by promoting the ubiquitination and degradation of the core circadian regulator BMAL1. *J. Biol. Chem.* 295:4696–4708. https://doi.org/10.1074/jbc.RA119.011280

Wang, A., A.E. Conicella, H.B. Schmidt, E.W. Martin, S.N. Rhoads, A.N. Reeb, A. Nourse, D. Ramirez Montero, V.H. Ryan, R. Rohatgi, et al. 2018. A single N-terminal phosphomimic disrupts TDP-43 polymerization, phase separation, and RNA splicing. *EMBO J.* 37:e97452. https://doi.org/10.15252/embj.201797452

Womac, A.D., J.F. Burkeen, N. Neuendorff, D.J. Earnest, and M.J. Zoran. 2009. Circadian rhythms of extracellular ATP accumulation in suprachiasmatic nucleus cells and cultured astrocytes. *Eur. J. Neurosci.* 30:869–876. https://doi.org/10.1111/j.1460-9568.2009.06874.x

Zhang, Mu, Shengyan Xiang, Heui-Yun Joo, Lei Wang, Kendra A Williams, Wei Liu, Chen Hu, Dan Tong, Joshua Haakenson, Chuangui Wang, et al. 2014. HDAC6 deacetylates and ubiquitinates MSH2 to maintain proper levels of MutSα. *Mol Cell.* 55:31–46. https://doi.org/10.1016/j.molcel.2014.04.028

Zheng, X., L. Boyer, M. Jin, J. Mertens, Y. Kim, L. Ma, L. Ma, M. Hamm, F.H. Gage, and T. Hunter. 2016. Metabolic reprogramming during neuronal differentiation from aerobic glycolysis to neuronal oxidative phosphorylation. *Elife.* 5:e13374. https://doi.org/10.7554/eLife.13374

Supplemental material

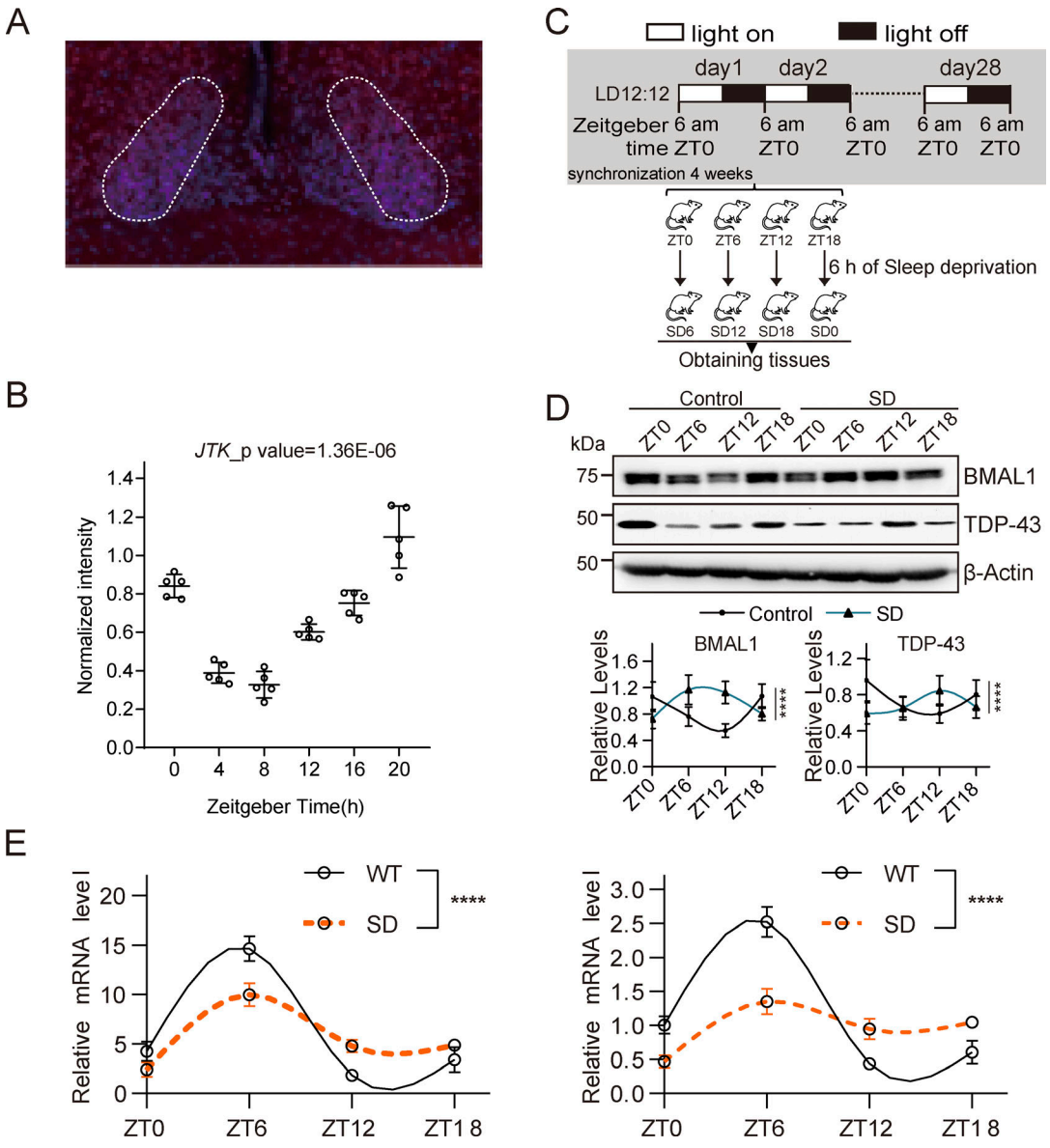

Figure S1. **Sleep deprivation alters the rhythmic expression of TDP-43 in the hypothalamus of mice (Related to Fig. 1). (A)** The dotted line indicates the edge of SCN of mice where was used to conduct the quantification. **(B)** The quantification of TDP-43 expression evaluated by immunofluorescence staining in the SCN region of male mice in Fig. 1. *JTK*_Cycle analysis confirms significant rhythmicity (P = 1.36E−06). Data are presented as mean ± SEM. **(C)** C57BL/6 mice were photoperiodic synchronized for 4 wk, and then placed in the sleep deprivation apparatus for 6 h started at different times (ZT0, ZT6, ZT12 and ZT18). They were sacrificed within the next 30 min and stripped of the brain tissues, together with the control mice. SD, sleep deprivation. **(D)** The expression of BMAL1 and TDP-43 in the hippocampus of SD mice was detected by western blotting and quantitated after densitometry. **(E)** In the SD model, the expression of *BMAL1* (left) and *TARDBP* (right) in the hypothalamus was detected using RT-qPCR and quantitated by comparing the two groups by two-way RM ANOVA. Data are presented as mean ± S.D. ****P < 0.0001. Source data are available for this figure: SourceData FS1.

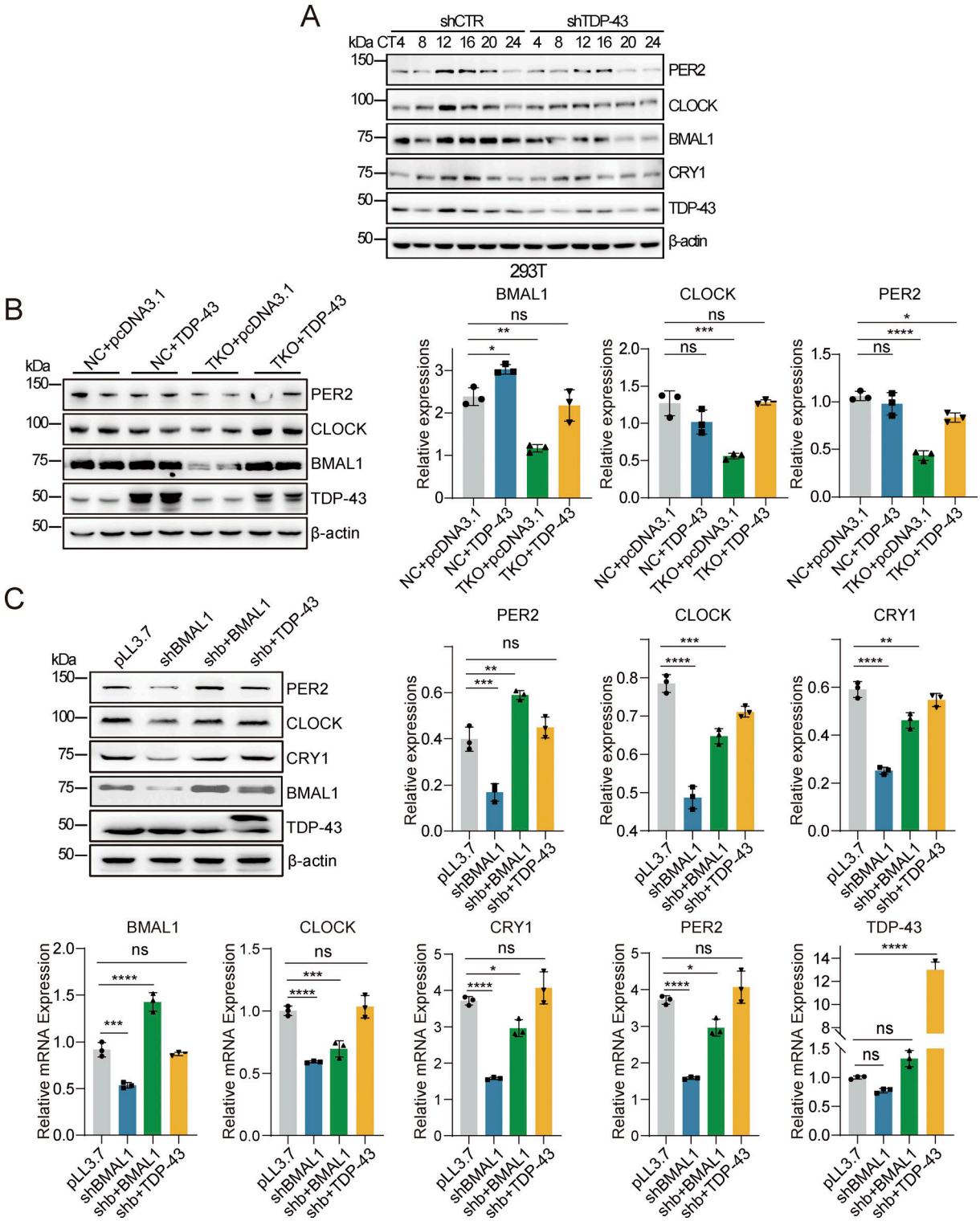

Figure S2. **TDP-43 regulates the expression of BMAL1, CLOCK, PER2, and CRY1 in cultured cells (Related to Fig. 2). (A)** Western blotting was used to evaluate the expression of BMAL1, CLOCK, PER2, and CRY1 at the indicated circadian times (CT) in HEK-293T cells transfected with an empty vector control (Con) or a short hairpin RNA vector targeting *TARDBP* mRNA (shTDP-43). **(B)** Western blotting showed the representative effect of ectopic expression of TDP-43 in the indicated groups on the expression of PER2, CLOCK, and BMAL1 proteins in TDP-43 knockdown HEK-293T cells (left), with quantification of the band density from each group (right). **(C)** Western blotting showed the representative effect of ectopic expression of TDP-43 or BMAL1 in the indicated groups on the expression of PER2, CLOCK, CRY, and TDP43 proteins in TDP-43 knockdown HEK-293T cells (left), with quantification (right). Effects of ectopic expression of TDP-43 or BMAL1 in the indicated groups on mRNA expression of *BMAL1*, *CLOCK*, *CRY1*, and *PER2* were determined using RT-qPCR (bottom). Data are presented as mean ± S.D. (n = 3) and compared by unpaired t test. *P < 0.05; **P < 0.01; ***P < 0.001; ****P < 0.0001. ns, no significance. Source data are available for this figure: SourceData FS2.

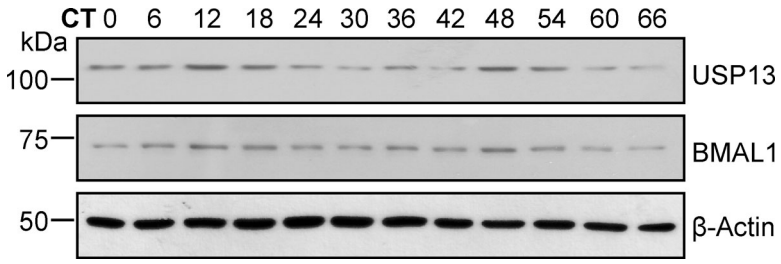

Figure S3. **USP13 exhibits rhythmic oscillations in expression in M17 cells (Related to Fig. 7).** The representative from three immunoblot experiments showed the rhythmic expression pattern of BMAL1 and USP13 at the indicated circadian times (CT) in M17 cells. Source data are available for this figure: SourceData FS3.

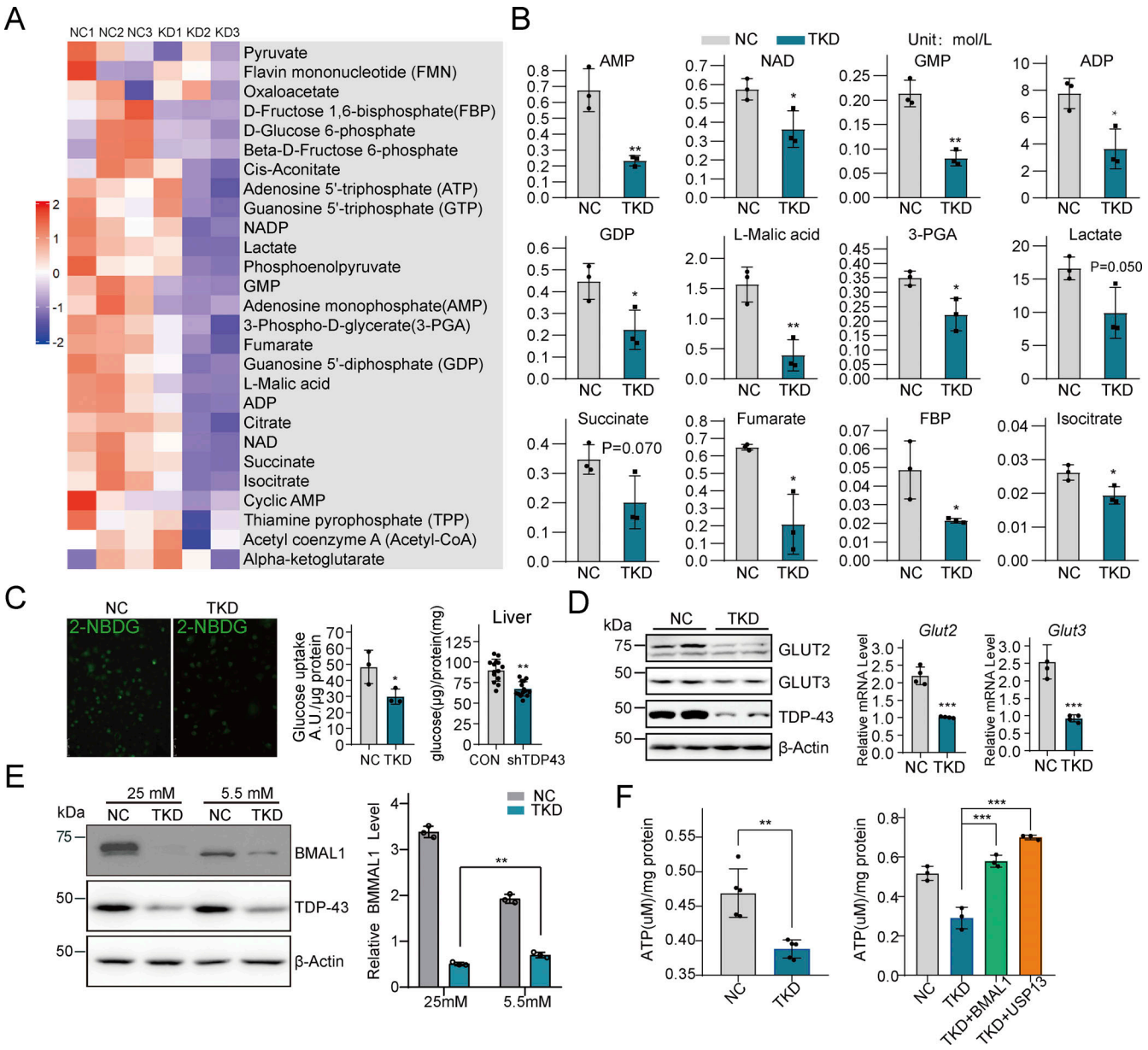

Figure S4. **TDP43 regulates cellular glucose uptake, glycolysis, TCA cycle, and energy production (Related to Fig. 8). (A)** M17 cells were infected with PX458/TDP-43$_{KO}$ (TKD) for 72 h and the cell lysates were sent to BGI company for metabolic flux analysis. Representative heatmap of the metabolism products. **(B)** Box plot of the products with significant differences. **(C)** HEK-293T cells were infected with PX458/TKD, and 48 h later, the medium was changed to sugar-free DMEM with 2-NBDG (200 μM) for 30 min. The green fluorescence of the cells was observed and quantitated (n = 3), and photos were taken under a microscope. The liver homogenates from the control AAV (CON) or AAV carrying TDP-43 shRNA (shTDP-43) icv-injected mice were performed for glucose concentration detection and quantitated (n = 15). **(D)** HEK-293T cells were transfected with PX458/TKD and extracted after 48 h. The cell lysates were analyzed using western blotting. RNA was extracted and performed for RT-qPCR. **(E)** TDP-43 depletion led to lower protein levels of BMAL1 in cells under high glucose conditions. Immunoblots showing the effect of TDP-43 knockdown on BMAL1 expression in M17 cells at the indicated glucose levels in the culture medium (Left), with quantification of the band density from each group (n = 3, Right). The data are presented as mean ± S.D. and quantitated (n = 3). **(F)** Ectopic expression of BMAL1 or USP13 significantly resorted the levels of ATP in the TDP-43 knockdown cells. ATP levels in indicated groups were measured in cells transfected with indicated DNA vectors. Data are presented as mean ± S.D. and compared with unpaired t test. *P < 0.05; **P < 0.01; ***P < 0.001. Source data are available for this figure: SourceData FS4.

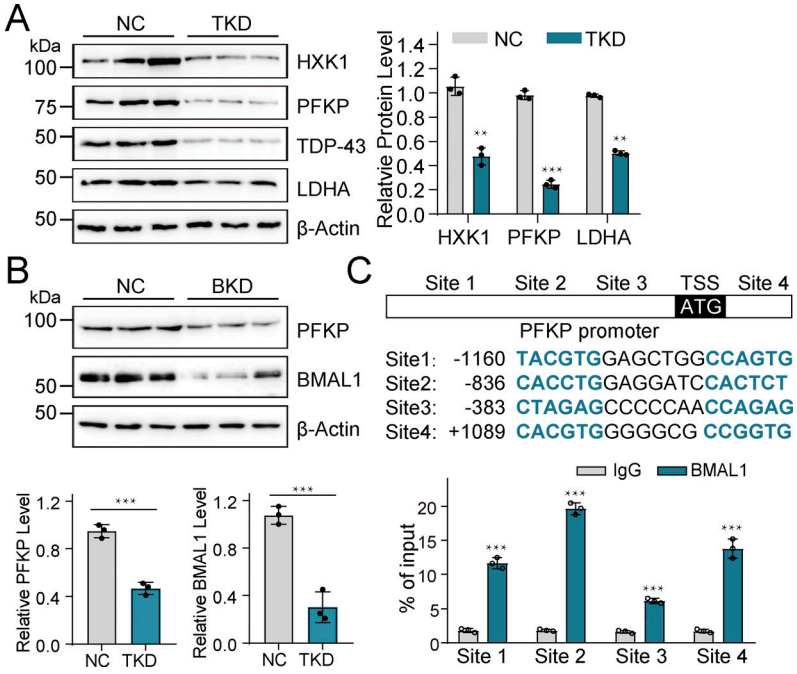

Figure S5. **TDP-43 controlsled neuronal glycolysis possibly by directly regulating the transcription of PFKP through BMAL1 (Related to Fig. 8). (A)** M17 cells were transfected with PX458 (NC) or PX458/TDP-43$_{KO}$ (TKD) for 48 h. The cell lysates were analyzed using western blotting with glycolytic kinase antibodies and quantitated. **(B)** M17 cells were transfected with PX458 (NC) or gene editor vector target BMAL1 designed as BMAL1$_{KO}$ (BKD) for 48 h. The cell lysates were analyzed using western blotting and quantitated. **(C)** Chromatin from M17 cells was immunoprecipitated with normal mouse IgG (IgG) or anti-BMAL1 (BMAL1). Quantitative PCR was used to detect IgG and BMAL1 antibody-enriched DNA fragments containing indicated four *BMAL1* binding consensuses (site1, site2, site3, and site4) in the *PFKP* promoter and quantitated. Data are presented as mean ± S.D. (n = 3) and compared with unpaired t test. **P < 0.01; ***P < 0.001. Source data are available for this figure: SourceData FS5.

Provided online are Table S1, Table S2, Data S1, and Data S2. Table S1 shows the primary antibodies used in this study. Table S2 shows the primers used for qPCR and ChIP in this study. Data S1 shows all source files for immunoblot experiments in excel file. Data S2 shows all source files for immunoblot experiments in PDF file.